CHAPTER 16

Photovoltaic, Photoelectronic, and Electrochemical Devices Based on Metal-Oxide Nanoparticles and Nanostructures

JUAN BISQUERT

Departament de Ciències Experimentals, Universitat Jaume I, 12071 Castelló, Spain

16.1. INTRODUCTION

Nanostructured metal-oxide films formed by an assembly of nanoparticles sintered over a conducting substrate provide a large internal area that can realize different functionalities. Titanium dioxide and several other metal-oxides nanostructures (e.g., ZnO, SnO_2, and Nb_2O_5) have the advantage of easy processing and low production cost and have the potential to replace existing devices based on more expensive technologies and to give rise to new applications. In recent years, such nanostructures have been amply investigated for several applications, such as dye-sensitized solar cells (DSC) (1) photoelectrochromic windows (2) and electrical paint displays (3), and protein immobilization (4).

The most intensively investigated metal-oxide nanostructured device is the DSC, which was discovered in 1991 by Michael Grätzel (1). The DSC is formed with a network of TiO_2 nanoparticles sensitized to the solar spectrum with a monolayer of dye molecules and a redox electrolyte (5–8). Overall, 11% efficiency of sunlight energy conversion to electricity has been achieved in DSCs (6) but their large-scale production has not yet been reached mainly due to technical problems such as evaporation of the liquid ionic conductor. The DSC has also paved the way for several applications of metal-oxide nanomaterials in other devices based on similar principles of operation. Examples are solid-state nanostructured solar cells (9), electrochromic devices for displays (10), ultraviolet light-emitting diodes (LEDs) (11), and nanostructured WO_3 and Fe_2O_3 electrodes for hydrogen production by photocatalytic splitting of water

Synthesis, Properties, and Applications of Oxide Nanomaterials, Edited by José A. Rodríguez and Marcos Fernández-Garcia

1.- Introduction

Nanostructured metal oxide films formed by an assembly of nanoparticles sintered over a conducting substrate provide a large internal area that can realize different functionalities. Titanium dioxide and several other metal oxides nanostructures (e.g., ZnO, SnO_2, Nb_2O_5) have the advantage of easy processing and low production cost and have the potential to replace existing devices based in more expensive technologies and also to give rise to new applications. In recent years such nanostructures have been amply investigated for several applications such as dye-sensitized solar cells (DSC),[1] photoelectrochromic windows[2] and electrical paint displays,[3] and protein immobilization.[4]

The most intensively investigated metal oxide nanostructured device is the DSC, discovered in 1991 by Michael Grätzel.[1] The DSC is formed with a network of TiO_2 nanoparticles sensitized to the solar spectrum with a monolayer of dye molecules, and a redox electrolyte.[5-8] 11% efficiency of sunlight energy conversion to electricy has been achieved in DSCs[6] but their large scale production has not yet been reached mainly due to technical problems such as evaporation of the liquid ionic conductor. The DSC has also paved the way for a number of applications of metal oxide nanomaterials in other devices based on similar principles of operation. Examples are solid-state nanostructured solar cells,[9] electrochromic devices for displays,[10] ultraviolet light-emitting diodes (LEDs),[11] and nanostructured WO_3 and Fe_2O_3 electrodes for hydrogen production by photocatalytic splitting of water.[12,13]Energy storage devices such as batteries and supercapacitors can also benefit in many respects from nanostructuring.[14]

In this chapter we will review the main characteristics of operation of these nanostructured devices and the results that have been achieved so far. We will consider several topics related to device operation: the characteristics of carrier transport in mesoscopic metal-oxide films, the means of coating and funcionalizing the surface, and the requirements of electrolytes and/or organic hole conductors that are usually employed for forming heterojunctions with nanostructured semiconductors. We will also highlight the physical properties of spatially regular nanostructures that are expected to give rise to new classes of devices. Quantum dots are small nanocrystalline particles where the strong confinement of the electron wavefunction provides discrete valence and conduction energy levels. The electrical and optical properties of quantum dots can be modified by controlling their dimension. Quantum dots can be assembled in highly ordered structures known as quantum dot solids, which may find, in the long term, applications in opto-electronic switches, LEDs, lasers, and solar cells.[15,16] Carbon nanotubes, discovered in 1991, have become a milestone in nanomaterials research. Several types of oxidic nanowires are accessible now[17] and have attracted wide scientific and technological interest owing to their novel structures and their potential applications in luminiscent devices and solar cells as well as in future nanoelectronic components, such as field-effect transistors (FETs), crossed junctions and actuators.

2.-General features of nanostructured photoelectronic and electrochemical devices.

The fundamental structure of a nanostructured device is shown in Fig.1. Semiconductor nanoparticles can be prepared by wet chemical methods that lead to colloidal nanocrystals present in dispersion. The colloidal nanocrystals are usually deposited, e.g. by screen printing, onto a glass or flexible plastic support covered with a conducting layer. The film is thermally treated to form an electronically connected array of nanoparticles. The nanostructured film is filled with an ionic conductor or hole-conducting medium that is contacted with a counterelectrode. The global structure of the device consists on interpenetrating bicontinuous phases in which the simultaneous transport of several carriers in the different phases and interfacial processes must be optimized.

Fig. 1. Scheme of an electroactive device formed by a nanoparticulate metal-oxide film and counterelectrode joined by an ionic conductor. Dark arrows indicate electrons pathways in the particulate network and in the external circuit, while the light arrow indicates ionic transport in the voids of the network up to the counterelectrode.

Electrons can be injected or extracted from the nanoparticulate film by external contact through the conductive support. Therefore the whole internal area of the nanoparticulate network is electronically addressable from the substrate. This very large active area for device function that is obtained by relatively simple preparation route is a main advantage of using metal oxide nanomaterials for electronic and electrochemical devices. In photonic applications the conducting substrate must be optically transparent, so that typically a thin layer transparent conducting oxide (TCO) such as indium-doped tin oxide or fluor-doped tin oxide over glass is used.

While electrons move across the metal oxide nanoparticualte network, the displacement of other charge carriers is needed in the medium filling the voids in the nanostructure of Fig. 1, i.e. the ionic conductor that is addressed from the counterelectrode. Liquid electrolytes have the advantages that they immediately form a perfect electric junction in the internal surface, and that they provide a large ionic conductivity and wide potential window of stability. However liquid electrolytes require efficient sealing which is a major drawback for the long term operation of devices. In general an all-solid state construction is preferable with solid electrolytes that allow for more compact and mechanically flexible device designs. Organic conductors are convenient media for hole conduction and heterojunction formation in nanostructured devices, since they can be deposited in solution form and fill the pores homogeneously. However the carrier mobilities are much lower than in inorganic semiconductors or liquid electrolytes. Recently, room temperature ionic liquids have emerged as an excellent medium for ionic carrier in nanostructured devices,[18,19] since they are non-volatile and non-flammable, have high thermal stability, and show excellent electrochemical properties, namely, high ionic conductivity and wide potential windows of operation.

Metal oxide nanoparticles are usually not intentionally doped and are therefore insulating. The high electronic conductivity required for addressing the internal surface from the substrate, is obtained by the injection of electrons in the nanoparticles. These electrons may be electrically injected from the substrate or photogenerated in the nanoparticles surface by sensitizers such as organic dyes or quantum dots.[20] (Doping of wide band-gap metal oxide nanoparticles for the sensitization to the visible spectrum has yielded so far very limited success, see below.) As a result the electron density varies by many orders of magnitude during device operation, see Fig. 8 below. Consequently a large density of negative charge is created in the nanoparticulate network, and in order to preserve overall charge neutrallity, the same amount of positive charge must occur in the surface of the nanoparticles, as it is suggested in Fig. 2a. In many cases to facilitate electron accumulation and transport by preserving the charge neutrality in the system is a primary function of the medium that fills the pores. Positive carriers in the ionic medium should have a sufficiently high mobility not to limit the displacement of the electrons in the nanostructure. In addition the average size of inorganic semiconductor units should be smaller (in the 10 nm range) than the Debye length, so that no internal electrical fields are built into one compact unit.[21] In contrast to bulk semiconductors, that show a special arrangement of energy levels in the space-charge region in the surface, in nanostuctured networks filled with a conductive medium there is no internal spatial distribution of the conduction band level in individual nanoparticles, and the whole nanostructure can be treated with a homogenous distribution of energy levels.

Let us discuss specific functions of carriers in some nanostructured devices with the configuration of Fig. 1:

(a) *Charge separation*. In DSC positive and negative carriers are created by sunlight in the molecules adsorbed at the nanoparticles surface. Electrons are injected in the metal oxide nanoparticles and travel all the way to the substrate. Meanwhile a conjugated carrier travels in the medium filling the pores towards the counterelectrode. This second carrier may be a redox ion which reacts at the counterelectrode. It may be also an electronic carrier in an inorganic or organic hole conductor. The net effect of the overall process is the collection of a negative carrier at the substrate of the nanoparticulate film and a positive carrier at the counterelectrode.

(b) *Charge recombination*. In the LEDs electrons are injected from the substrate of the

nanoparticulate film (the cathode) and holes are injected from the electrode contacting the other medium (the anode). Both carriers should travel in their respective media and meet at the surface of the nanostructure, to recombine radiatively emitting light.

(c) *Charge accumulation*. By modifying the carrier density in the nanostructure, the chemical potential of such carrier is changed significantly. With accumulated charge the device can supply a voltage, and an electric current when the external circuit is connected to some load. This is the basic principle of operation of intercalation batteries and electrochemical supercapacitors.[22]

A useful scheme for describing the transport and charge-transfer properties in nanostructured devices is the transmission line model shown in Fig. 2. This model has been developed[23-25] for the interpretation of impedance spectroscopy results and has found wide application for understanding and characterizing the properties of electrochemical nanostructured devices[26-30] and DSC.[31-33]

Fig. 2. (a) Electron energy diagram of a nanostructured metal oxide electrode in contact with a redox electrolyte (or hole conducting medium), illustrating the electrochemical potential of electrons E_{Fn} (Fermi level) when a potential V is applied to the substrate, and assuming that conduction band energy (E_c) remains stationary with respect to the redox level, E_{redox}. (b) The equivalent circuit (transmission line model) for a small periodic ac perturbation, that contains the transport resistance along the metal oxide nanoparticles, r_1; the resistance in the hole/ion conducting medium, r_2; the charge transfer resistance at the metal oxide/electrolyte interface, r_3; and the capacitance for charge accumulation in the metal oxide particles and/or surface, c_3. (c) Distribution of electrons injected in the nanostructured film from the substrate, for the case in which the diffusion length is much larger than the nanoparticulate film thickness, $L_n > L$, and for the opposite case, $L_n < L$, as indicated. n_0 is the equilibrium concentration.

In the representation of Fig. 2a, it is assumed that the medium filling the voids in the nanostructure, possesses a large conductivity and a large carrier density (e.g., a liquid electrolyte). For this reason, the Fermi level/redox potential in the hole-conducting medium will not be significantly changed when the potential between the contacts is modified. The variation of potential mostly causes a displacement of the Fermi level, E_{Fn}, inside the metal oxide nanostructure, from the equilibrium value, which equals the redox potential of the electrolyte, $E_{F0} = E_{redox}$, towards the conduction band. The gradient of the Fermi level indicates the direction of electron diffusion. The electron density decreases with the distance from the substrate due to charge transfer events from the semiconductor to acceptor species in solution.

In the transmission line model of Fig. 2b there are different processes represented. In general the resistances describe carrier flux with respect to a difference of electrochemical potential, while capacitors represent carrier storage. The longitudinal resistance r_1 relates the local carrier flux to the variation of E_{Fn} with distance in the nanoparticulate structure, and corresponds to the transport resistance, i.e. it is the inverse of the electronic conductivity.[25] Similarly, r_2 describes the transport or carriers in the ion- or hole-conducting medium. In the situation indicated above for a liquid electrolyte, r_2 will be very low and provides no limitation for the device operation, however in the case of organic conductors r_2 cannot be neglected. The resistance r_3 describes the carrier flux by charge-transfer between the two phases and corresponds to recombination flux in DSC. Properties of the capacitance of the nanostructured network will be commented in the next Section.

In the characteristic structure of the transmission line of Figure 2b, the transport resistances, distributed in the spatial direction of each transport channel, are continuously interrupted by

inter-phase elements $r_3 c_3$. This combination represents the physical current flow, ie. a carrier in the nanoparticle has a probability to move forward or to drop in the electrolyte. For the efficient operation of a device, the different elements governing transport and recombination must be correctly taylored and balanced. For example in the presence of a large recombination flux (low r_3) and low conductivity (large r_1), carriers injected from the TCO will not move far from the substrate, and in this case a large part of the device will not be operative.

There are two main time constants that describe more precisely such characteristics of a device: the lifetime of the carriers, τ_n, and the transit time over the film thickness L. If the carrier diffusion coefficient is D_n, the transit time is (up to a numerical constant of order 1)

$$\tau_{tr} = \frac{L^2}{D_n} \tag{1}$$

The relationship between the time constants can be written

$$\frac{\tau_{tr}}{\tau_n} = \left(\frac{L}{L_n} \right)^2 \tag{2}$$

in terms of the diffusion length, that is defined as

$$L_n = \sqrt{D_n \tau_n} \tag{3}$$

When the quotient in Eq. (2) is <<1, the carriers have time to travel the entire thickness of the layer before recombining, which is an essential requirement for efficient solar cells. The diffusion length also gives a measure of the extent of the penetration of the carriers that are voltage-injected at the boundary of the layer. Figure 2c indicates two extreme situations. The right boundary is considered completelly blocking. In the case when the diffusion length is much larger than the film thickness, the carriers are nearly homogeneously distributed in the available volume. On the other hand in the high-reactivity case $L_n << L$, the carrier concentration decays rapidly close to the injecting boundary of the porous structure.

3.-Measurement techniques for characterization of nanostructured photoelectronic and electrochemical devices.

The most basic characteristic of a solar cell is the steady-state performance given by the current density-potential curve at fixed incident illumination. This curve gives the main parameters determining the solar cell performance: the short-circuit photocurrent (I_{sc}), the open-circuit potential (V_{oc}), and also the fill factor (FF), which describes the quality of the diode behaviour of the solar cell and determines the power output of the solar cell at the point of maximum power operation. Steady-state characteristics are obviuosly important for the performance of other devices such as LEDs. However, it is usually difficult to extract detailed device properties only from steady-state measurements. There are two main issues for investigation: (i) The determination of quantities such as the diffusion coefficient and the lifetime of the different carriers, which govern the fundamental electronic processes occurring in the device function. These time constants are also crucial characteristics for devices that require fast switching or fast power supply, such as elecrical paint displays and supercapacitors, respectively. (ii) The separation of different effects in the global device response, for their separate optimization. These two issues can be addressed with a range of measurement methods in combination with rational variation of the device components.

The time constants mentioned above are obtained by specific small perturbation kinetic techniques that do not modify the steady state over which they are measured. Examples of the techniques are intensity modulated photocurrent spectroscopy (IMPS),[34-38] intensity modulated photovoltage spectroscopy (IMVS),[39] and small amplitude time transients.[40-44]

Fig. 3. (a) Simulation of the diffusion-recombination impedance with reflecting boundary condition. Parameters $R_1 = 10^2\ \Omega/\mathrm{cm}^2$, $R_3 = 10^3\ \Omega/\mathrm{cm}^2$, $C_\mu = 5\times10^{-6}\ \mathrm{F/cm}^2$. Shown are the frequencies in Hz at selected points, the characteristic frequency of the low frequency arc (31.8 Hz, square point), related to the angular frequency ω_3, the low frequency resistance, and the characteristic frequency of the turnover from Warburg behaviour to low frequency recombination arc (318 Hz, square point), related to the angular frequency ω_1. (b) Shows an enlargement of (a). (c) The case $R_1 = R_3$. (d) The case $R_3 << R_1$.

Electrochemical impedance spectroscopy[24,31-33,45-47] measurement of nanostructured devices has the advantage of providing a determination of the time constants as well as spectrally separating different internal contributions of the overall device operation. However, when there are different processes acting in combination in a nanostructured device, the interpretation of impedance spectroscopy results requires appropriate models for extracting the relevant information. As an important example we discuss the impedance model of diffusion and reaction of the carriers in nanostructured electrodes, which has the following expression[24]

$$Z = \left(\frac{R_1 R_3}{1 + \mathrm{i}\omega/\omega_3} \right)^{1/2} \coth\left[(\omega_3/\omega_1)^{1/2} (1 + \mathrm{i}\omega/\omega_3)^{1/2} \right] \tag{4}$$

where ω is the angular frequency of the perturbation. In Eq. (4) we use the total resistances for transport $R_1 = Lr_1$ and recombination $R_3 = r_3/L$, and the characteristic frequencies $\omega_1 = {\tau_{tr}}^{-1} = 1/R_1 C_3$ and $\omega_3 = {\tau_n}^{-1} = 1/R_3 C_3$, where $C_3 = Lc_3$ is the total capacitance. Eq. (2) can be restated as

$$\frac{R_1}{R_3} = \frac{\omega_3}{\omega_1} = \left(\frac{L}{L_n} \right)^2 \tag{5}$$

The impedance pattern of Fig. 3a corresponds to the case $R_1 << R_3$, i.e., the transport (diffusion) resistance is much lower than the recombination resistance. In this case, that indicates a large diffusion length, the impedance spectra show a small feature at high frequency which is the Warburg (diffusion) impedance, with an inclination of 45º, see Fig. 3a. At lower frequencies a large arc is obtained, which is due to the combination of charge-transfer resistance and capacitance. In contrast, in the high-reactivity case, $R_3 << R_1$, or in other words $L_n << L$, the impedance pattern changes to that of Fig. 3d, which is known as the Gerisher impedance. Fig. 3b shows the spectral shape obtained in the transition between the two previous extreme situations, i.e. $L_n \approx L$.

A representative measurement of impedance spectroscopy of nanostructured TiO_2 electrodes is shown in Fig. 4.[48] The impedance pattern of Fig. 3a is well realized, indicating that electron transport across the film length is faster than the rate of recombination. From such spectra the different time constants τ_n and τ_{tr} can be obtained, and also the electron conductivivity and diffusion coefficient. These quantities have been systematicaly determined as a function of bias potential.[26,31]

Fig. 4. Impedance spectroscopy of a 8 μm thick film of nanostructured TiO_2 (10 nm nanoparticles anatase) in aqueous solution at pH 2, with –0.250 V bias potential vs. Ag/AgCl under UV illumination. The line is a fit to the model of Eq. (4).[48]

It is interesting to mention the impedance behaviour of nanostructured films in which there is no charge-transfer at all. This occurs in an inert electrolyte that realizes charge shielding but lacks any electron acceptors, what is a fundamental requirement of several capacitive devices such as Li-batteries and supercapacitors. The model obtained with $R_3 \to \infty$ in Eq. (4) is shown in Fig. 5. The impedance of unreactive porous electrodes shown in Fig. 5 is characterized by a capacitive domain at low frequencies and a "Warburg" part at high frequencies that relates to the transport of the species flowing in the nanostructure (or in the electrolyte) in order to charge the whole film. For a perfect capacitor in the transverse branch, the impedance reduces to the classical transmission line of de Levie[49] for porous electrodes.[50] But the capacitive response in many real systems does not show a perfect capacitor and is better described by a constant phase element (CPE),[51,52] with admittance

$$y_3 = q_3(\mathrm{i}\omega)^{\gamma_0}; \quad q_3 = Q_3 / L \tag{6}$$

Equation 6 reduces to the perfect capacitor in the particular case $\gamma_0 = 1$. In general the CPE in the transverse element of the transmission line, changes the slopes of the Warburg and capacitive lines of the impedance spectra, depending on the extent that the exponent γ departs from the value of 1 of the ideal capacitor.[23] The deviations from the ideal model in the low and high frequency lines have a common origin in the dispersive element Q_3, as seen in the example of Figure 5 for $\gamma_0 = 0.8$. Hence the slopes are related by the high frequency line having an exponent $\gamma_0 / 2$, while the low frequency line is the full CPE, i.e., the latter exponent doubles the former one, as discussed in Ref. [23]. This means that even in the presence of frequency dispersion the behaviour of a porous electrode can be spectrally recognized by impedance measurements. An experimental instance of frequency dispersion can be observed in the less than 45º inclination of the spectrum of Fig. 4 at high frequency, and another case is discussed below in Fig. 16.

Fig.5. Simulation of the impedance spectra for the transmission line model indicated in the scheme with $R_1 = 20\,\Omega$, $Q_3 = 5\,\mathrm{mF\ s}^{1-\gamma_0}$, and two values of the CPE exponent γ_3 as indicated in the left diagram. Also indicated in the rigth diagram is the inclination of the low and high frequency lines, in radians.

The spectra of the type of Fig. 5 are very well realized in carbonaceous supercapacitors, for example.[53] Independently of the presence of frequency dispersion, the spectra of Fig. 5 indicate important limitations for nanostructured devices which large charge storage and fast transient response demands. In these devices the amount of energy storage is governed by the total capacitance that is $C_3 = Lc_3$. If the specific capacitance of nanoparticles c_3 has been optimized, increasing the device capacitance requires increasing film thickness. However one must take into account the charging region in the frequency domain that is observed in Fig. 5 with the inclination $\leq \pi/4$. This region is onset at times shorter than $\tau_{tr} = L^2 / D$. Therefore increasing the film capacitance with larger thickness has the adverse effect of increasing (quadratically) the operation time of the device. Even if a highly conducting porous medium is used (such as carbon nanoparticles), the transient response will be governed by electrolyte diffusion coefficient. As an example $D = 10^{-5}\ \mathrm{cm^2 s^{-1}}$ and $L = 10\,\mu\mathrm{m}$ gives a limitation of $\tau = 0.1\,\mathrm{s}$ for device operation.

In the situations discussed so far we have focussed on diffusive transport of carriers, granted that a large conductivity that anihilates any local space charge and shields electrical fields is available in at least one of the interpenetrating bicontinuous phases. Let us mention the other

limiting case, consisting of basically *insulating* phases where carriers can be injected by suitable contacts. In the absence of intrinsic conductivity, application of a voltage requires the injected carriers to redistribute themselves in order to maintan a local field that drives the transport (usually by predominant drift mechanism). This is the space-charge-limited current transport[54] which is typically found, for example, in organic LEDs[55] and in some organic solar cells.[56]

It is important to recognize that nanostructured devices are characterized by the abundance of interfaces of different kinds, which must be controlled for facilitating the proper device function. In particular nanostructured solar cells are usually largely determined by the competition of kinetics of charge transfer at several interfaces,[57] which governs the selectivity of contacts that is required in photovoltaic devices.[7,58] The main (and larger) interface is that between the nanostructured metal oxide and the ionic/hole conductor, as it has already been described in terms of the resistance R_3 above. This interface is crucial for the diode characteristic of the solar cells[47] and usually receives a great deal of attention when material and device properties are selected. However, additional contacts should be correctly engineered to avoid unwanted resistances or internal short-circuits. Figure 6 shows as an example additional impedances that may occur in the model of Fig. 2b.[59] Z_{c1} is an impedance at the electron injecting/extracting contact, that is determined by the interfacial barrier formed between the metal oxide and the conductive substrate. It is usually desired that this interface forms an ohmic contact in which $Z_{c1} \approx 0$ (short-circuit in Fig. 2b) so that dissipative losses are avoided in device operation. Figure 6 also shows the impedance between the substrate and the ionic/hole conducting medium. Ideally one usually needs that this impedance is totally blocking for electron transfer, i.e. $Z_{c2} \to \infty$ (open-circuit in Fig. 2b), to avoid the metal oxide nanostructure becoming short circuited by the direct electronic pathway between the two external contacts across the ionic conductor. In DSC with an organic hole conductor the reactivity of the substrate is large and it must be pre-treated with a thin metal oxide layer that blocks the charge transfer to the hole-conducting medium while maintaining good electron-injection properties towards the nanoparticles. Finally a resistance Z_{c3} relates to the facility of charge transfer at the counterelectrode. In summary, it should be appreciated that the proper device function requires the materials determining the three contact impedances in Fig. 6 to be treated for reducing the equivalent circuit of Fig. 6 to that of Fig. 2b, which drives the current through the nanostructure area without side effects. We should mention also that in large area devices with a transparent conducting substrate, the transport of electric current along the TCO substrate often introduces major resistive losses.

Fig.6. Transmission line equivalent circuit model, based in Fig. 2b, and showing in addition the impedance at the metal oxide/subtrate interface, Z_{c1}, the impedance at the electrolyte/substrate interface, Z_{c2}, and the impedance at the electrolyte/counterelectrode interface, Z_{c3}.

Let us describe other techniques that provide relevant characteristics of the metal-oxide nanostructured films. The electrochemical transistor configuration, Fig. 7a, uses a conducting substrate that is divided in two separated regions, bridged by the nanostructured film,[60] and allows to determine the electronic conductivity as a function of electrode potential. The two regions of the conducting substrate can be controlled as independent working electrode, so that the Fermi level in the film can be governed with a bias $U_1 \cong U_2$, Fig. 7b, while maintaining a small potential difference between the two sides, $\Delta U = U_2 - U_1$, which causes a current flow ΔI between WE_1 and WE_2 that enables to measure the electronic conductivity, σ. This method has been applied in a number of metal-oxide nanostructured films.[60-63]

Fig. 7. Electrochemical transistor measurement configuration. The conducting substrate over which the film is deposited is divided in two regions, separated by an insulating gap. The separated regions serve as two working electrodes WE_1 and WE_2. (b) Equivalent circuit of the electrochemical transistor configuration. When WE_1 and WE_2 are shorted the film can be operated as in normal electrochemical cell with potential U_{bias}. The two working electrodes can also be operated independently with potentials U_1 and U_2 with respect to the reference electrode (RE).

Figure 8 shows the 9-order of magnitude change of the electronic conductivity of nanocrystalline TiO_2 films immersed in solution when the Fermi level is displaced towards the conduction band. This figure illustrates the *global* transformation from insulator to conductor of the films by external potentiostatic control that is a genuine effect of the nanocrystalline structure, in comparison with the bulk material counterpart, which conductivity can only changed in the surface.

Fig. 8. Electronic conductivity in nanostructured TiO_2 electrodes in solution at pH 2 as a function of the electrode potential, obtained by two different measurement methods as indicated.[60]

Next we consider the special features of the capacitance of nanocrystalline films and its relationship to the density of states (DOS).[64] There are two main basic mechanisms of accumulating charge with respect to voltage in electrochemical systems. The first one, is that occurring in a standard dielectric capacitor where energy is stored in the electrical field, related to spatial charge separation. This capacitance is ubiquituous at interfaces with space charge such as Schottky barriers and Hemlholtz layers. In the other mechanism, which is predominant in many nanostructured and intercalation systems, the energy storage is associated with a change of the chemical potential of the accumulated species. When a voltage variation dV is applied to the conductive substrate of a nanostructured metal-oxide film, and the Fermi level is displaced homogeneously in the film as $dE_{Fn} = -qdV$ (where q is the elementary charge) the electron density changes by a quantity dn. The electrochemical capacitance (per unit volume) relates the change of concentration of electrons, n, to the change of electrochemical potential

$$C_\mu = q\frac{dn}{dE_{Fn}} \tag{7}$$

Assuming that the conduction band potential is stationary, the Fermi level inside the TiO_2 nanostructure is displaced towards the conduction band, i.e., the change of electrochemical potential implies a change of the chemical potential of electrons: $dE_{Fn} = d\mu_n$. Equation (7) gives a purely chemical capacitance.[64] If $g(E)$ is the DOS in the bandgap, the chemical capacitance is obtained integrating all the contributions of occupied states

$$C_\mu = q^2 \int_{-\infty}^{+\infty} g(E)\frac{df}{dE_{Fn}}dE \tag{8}$$

where f is the Fermi-Dirac distribution. To a good approximation near room temperature,[65] Eq. (8) takes the form

$$C_\mu(E_{Fn}) = q^2 g(E_{Fn}) \tag{9}$$

It is therefore found that the chemical capacitance is proportional to the DOS. The interpretation of Eq. (9) is that the extent of charging related to the perturbation dV

corresponds to filling a slice of traps at the Fermi level. A common finding in nanostructured TiO_2 is an exponential distribution of localized states in the bandgap as described by the expression

$$g(E) = \frac{N_L}{k_B T_0} \exp\left[(E - E_c)/k_B T_0\right] \tag{10}$$

Here N_L is the total density and T_0 is a parameter with temperature units that determines the depth of the distribution.

One convenient method of measuring the chemical capacitance is the standard cyclic voltammetry technique (CV),[66] that monitors the current injected in the film as the potential varies at a constant speed, $s = dV/dt$. The electronic current flowing into a unit volume is

$$j = -q\frac{dn}{dt} = q^2 \frac{dn}{dE_{Fn}} \frac{dV}{dt} = sC_\mu \tag{11}$$

Hence, $C_\mu(E_{Fn})$ is measured directly by cyclic voltammetry. Figure 9c illustrates that the shape of a CV reveals directly the shape of the exponential DOS of Eq. (10).

Limitations by transport that cause the film to depart from equilibrium during the measurement, distort the shape of CV along the voltage axis, while the presence of cathodic charge-transfer makes the anodic (positive current) peak much smaller than the cathodic (negative current) one.[66] However the quasi-equilibrium condition of the film can be recognized by an invariant shape of the CVs at different scan rate and a current that is proportional to s.

The CV method has been applied in several works for obtaining detailed information of nanostructured TiO_2 energy levels under different surface treatments[45,67] or electrolytes.[68] This method is also important for stuying the redox properties of organic molecules attached in the TiO_2 surface, as in the case of viologen molecules[27] and proteins.[4,69] Provided that there is fast electron exchange between the semiconductor and the attached species, the functionalized electrode will show and excess of capacitance in the CV corresponding to the redox capacitance of the molecular species, in comparison with the bare TiO_2 electrode.

Fig. 9. The left column shows the schematic energy diagram of a nanostructured semiconductor under application of a potential that rises homogeneously the Fermi level in the film for the case of (a) stationary energy levels and (b) shift of the energy levels by modification of the Helmhotz potential at the nanoparticles surface during electron injection. The rigth column shows the corresponding CVs for an exponential distribution of bandgap states in the nanoparticles.

It has already been discussed that for maintaining charge neutrality into a nanostructured film it is required that the increasing electron charge in the nanoparticles be accompanied by positive ion charge at the semiconductor/electrolyte interface. As shown in Figure 9b, surface charging at increasing electron density in the nanoparticulate network changes the potential difference in the Helmholtz layer, producing an upward shift of the semiconductor energy levels.[70] The combined effect of electron accumulation and partial band unpinning can be accounted for by a constant Helmholtz capacitance, C_H, connected in series to the chemical capacitance, C_μ, so that the total electrochemical capacitance becomes

$$C = \left(C_\mu{}^{-1} + C_H{}^{-1}\right)^{-1} \tag{12}$$

Hence when the exponentially increasing C_μ becomes larger than C_H, the CV flattens to a constant value, Fig. 9d, in consonance with the fact that the band shifts simultaneously with the displacement of the Fermi level, with a smaller rate of gain of electron density in the

nanostructure.

4.-Dye-sensitized solar cells

Since the first report[1] of 1991 a major scientific and technical research effort has been devoted to the DSC (see the review articles[5-8]) which now constitutes a credible chemical alternative to the already established silicon and thin film photovoltaic technologies. In addition the research on DSC has revealed many important general aspects of the principles of operation of nanostructured devices. In the following we revise some of the properties of the DSC that have emerged from the research. Related devices will be described in the next Section.

The main electronic processes occurring in a DSC are shown schematically in an energy diagram in Fig. 10. The initial step of operation is the excitation of the dye molecules by absorption of sunlight. Ruthenium polypyridyl complexes have proved to be the most efficient TiO_2 sensitizers, with the *cis*-$RuL_2(SCN)_2$ (L=2,2'-bipyridyl-4,4'-dicarboxylic acid) dye (N3 dye) demonstrating incident photon-to-electron conversion efficiencies (IPCEs) of up to 85% in the spectral region 400-800 nm corresponding to almost unity quantum yield (electrons per absorbed photon). The next steps produce the separation of the excitation of the dye into carriers in the different transport materials: the injection of an electron from a photoexcited dye to the conduction band of the TiO_2, and the transfer of an electron from the ionic conductor to the dye.[71] The former process is usually completed within 200 ps, and the later, the regeneration of the oxidized dye, is completed within the nanosecond time scale. When the charge carriers have been transfered to the separate electron and ionic/hole conducting media, they propagate in their respective media towards the outer contacts. Electron transfer at the TiO_2/TCO interface is not thought to be a significant limiting factor in the DSC. On another hand the oxidized form of the redox carrier must be reduced at the counterelectrode, usually Pt-catalized TCO, as shown by the element Z_{c3} in the equivalent circuit of Fig. 6.

Fig. 10. Schematic energy drawing of the electron (arrows) and hole (dashed arrows) transfer processes at the metal-oxide/dye layer/hole transport material in a DSC. The grey boxes indicate available electronic states, E_{F0} is the dark Fermi level, E_{Fn} is the Fermi level of electrons accumulated in TiO_2 nanoparticles, and E_c is the lower edge of the metal oxide conduction band. (1) Photoexcitation. (2) Electron injection from lowest unoccupied molecular orbital (LUMO) of the dye to metal oxide conduction band levels. (3) Electron diffusion in metal oxide nanostructure. (4) Electron extraction at the TCO. (5) Hole transfer from highest occupied molecular orbital (HOMO) of the dye to hole transport material (HTM) HOMO. (6) Hole diffusion in HTM. (7) Electron transfer from the Pt counterelectrode to the oxidised ionic species, or to HTM HOMO. (8) Electron transfer from metal oxide to HTM and to (9) dye HOMO.

Nanostructured TiO_2 used in DSC is typically composed of anatase particles prepared by the hydrothermal method.[63] They exhibit predominantly a bipyramidal shape, the exposed facets having (101) orientation, which is the lowest energy surface of anatase. The density of electronic states (DOS) in these nanostructures has been investigated using a variety of methods: cyclic voltammetry, as described above,[66] impedance spectroscopy,[31] voltage-decay charge-extraction method,[72,73] and potential step-current integration (chronoamperometry).[63,74] All of these methods are based on the determination of the chemical capacitance. The results[31,66,72-74] agree in the existence of an exponential distribution of bandgap states in nanostructured TiO_2, which is indicated in Fig. 11b. However, the origin of such bandgap states, and the influence of the surrounding media in the energetics of the electrons, remains unclear.

Fig. 11. (a) Schematic energy diagram of electronic processes in a TiO_2 nanoparticle in a dye-sensitized solar cell. E_{F0} shows the position of the Fermi level in the dark, which is equilibrated with the redox potential (E_{redox}) of the iodide/triodide couple. E_{Fn} is the quasi-Fermi level of electrons accumulated in the nanoparticles and E_C

is the conduction band energy. The shaded region indicates the bandgap states that are occupied with electrons (zero-temperature approximation of Fermi-Dirac distribution). The arrows show a sequence of processes in the following order: thermal promotion of an electron from a bandgap localized state in the bulk of the nanoparticle, to the conduction band; electron diffusion in the conduction band states; trapping of an electron in a surface state; electron transfer from the surface state to the acceptor triiodide ions in solution, which form a distribution with an effective gaussian density of states, indicated in the right, with halfwidth λ, the reorganization energy.[75] (b) Quantitative diagram of the thermal occupation at temperature $T = 300\,\mathrm{K}$ (thick line) of an exponential DOS in the bandgap (thin line) with $T/T_0 = 0.25$, as determined by the Fermi-Dirac distribution function (dashed line).

Let us look in more detail at the electronic processes occurring in the TiO_2 nanoparticle in the operation of the solar cell, following the schematic diagram of Fig. 11a. Electrons photoinjected from the surface sensitizer accumulate in the TiO_2 nanostructure. Therefore, the electrochemical potential of the electrons in the TiO_2 nanoparticles (the quasi-Fermi level, E_{Fn}) increases. At open-circuit conditions, provided that there is sufficient electronic conductivity (produced by the injected electrons themselves, Fig. 8), the Fermi level tends to be homogeneous in the nanostructure, and it produces an increase of the potential at the substrate, which is the photovoltage, V_{oc}, typically 0.8 V. The number of electrons, determining the photovoltage, is established by dynamic equilibrium between the rate of gain of electrons (photoinjection) and the rate of their loss, which is caused by charge transfer at the surface of the nanoparticles.

The role of the redox mediator in the photovoltaic process is to reduce the oxidized dye, but the oxidized component of the redox couple (I_3^-) is present in the pores and is able to accept electrons from the TiO_2. In addition some of the injected electrons return to the oxidized dye molecules before they can be regenerated by the ionic conductor. These two charge transfer processes constitute the electron recombination in the DSC. It is important to recognize that the efficiency of the DSC relies on a strong differential kinetics of the redox couple at two interfaces.[57] The transfer of electrons in the TiO_2 to oxidised ionic species must be slow, to facilitate electron storage, whereas electron transfer to the same species should be very fast at the counterelectrode, avoiding the requirement of a significant overpotential for drawing current (typically 15 mA cm^{-2}) from the cell under solar illumination. In Fig. 11a the recombination process is suggested for an electron that is trapped at a surface state in the bandgap and subsequently is transfered to the fluctuating energy levels of the oxidized species in the electrolyte, following the Marcus-Gerisher model for electron transfer, as applied to DSC.[75-77]

Since the operation of the DSC is largely governed by the relative rates of several charge transfer steps, the energetics of the metal-oxide nanoparticle, relative to the molecular species in the surface and in solution, must be carefully controlled. There are several ways to modify the position of the semiconductor energy levels. Due to the fact that there is no internal bandbending in individual nanoparticles,[21] modifying the potential difference at the oxide/electrolyte interface *globally* displaces the energy levels suggested in Fig. 11a with respect to the redox potential E_{redox}. An *upward shift* (to more negative potentials) of the energy levels in the semiconductor in the equilibrium condition of the solar cell, produces and increase of V_{oc}, because at the same electron density the E_{Fn} lies higher up, with respect to E_{redox}. These shifts can be achieved with agents such as 4-*tert*-butylpyridine (TBP) or ammonia that depronotate the TiO_2 surface.[39] The TiO_2 energy levels can also be controlled by adsorption of a series of organic molecules with different dipole moments. The change of the conduction band position is illustrated by the displacement of the conductivity plot along the potential axis shown in Fig. 12 when different molecular modificants are attached to the TiO_2 surface.[78] Incidentaly this plot shows the sensitivity of the conductivity measurement, described in Fig. 7, to the changes of the TiO_2 surface, an effect that can be used for sensing as commented later on. In the DSC a negative shift of the conduction band, however, hampers electron injection from the excited sensitizer,[79]

and it has been found that increasing the V_{oc} by these means usually produces a decrease of the photocurrent.[39] In addition to these modifications, a light-induced shift of the conduction band at high electron density is possible as discussed before in Fig. 9b.

Fig. 12. Conductivity plot of a bare, mesoporous TiO_2 film and molecular modified films with electrochemical deposited 4-methoxybenzenediazonium tetrafluoroborate (oab) and 4-cyanobenzenediazonium tetrafluoroborate (cab). Adapted with permission from S. Ruhle, M. Greenshtein, S.-G. Chen, A. Merson, H. Pizem, C.S. Sukenik, D. Cahen and A. Zaban, J. Phys. Chem. B **109**, 18907, Copyright 2005 American Chemical Society.

Another route for improving the photovoltage in a DSC is to block the transference of the photoinjected electrons to the acceptor species in solution, provided that the blocking agents do not significantly decrease electron injection from the dye molecules. This involves the introduction of an insulating layer in the TiO_2 surface that is exposed to the solvent,[80] which faces the complexity of mutual effects between the insulating layer and the dye, or with absorbants (e.g. amphiphilic molecules containing carboxylic or phosphonic end groups) that form a more compact monolayer, comprised of the dye and coadsorbent, than the dye monolayer alone.[81] Recently, it was found[45] that the coadsorption of 4-guanidinobutyric acid with the K-19 sensitizer (Ru (4,4′-dicarboxylic acid-2,2′-bipyridine) (4,4′-bis(p-hexyloxystyryl)-2,2′-bipyridine)$(NCS)_2$) remarkably increases the photovoltage, by a simultaneous shift of the TiO_2 conduction band and blocking of the recombination, without suffering significant decrease of the photocurrent. It has also been observed that one of the factors controlling the charge recombination dynamics in DSC is the spatial separation of the dye cation HOMO from the TiO_2 surface.[82]

Composite material nanoporous electrodes formed by two materials that differ by their conduction band potential have been tested to improve the DSC performance.[74,83-89] Arranging these materials in the correct geometry is expected to drive the electrons in the direction of the material having the lower conduction band. A coated matrix design, denoted as core-shell, is achieved by the use of ultrathin ($\leq$ 1 nm) conformal coating layers deposited onto the surface on the syntered nanocrystalline metal oxide films. This design ensures free electrons diffusion to the current collector by avoiding the introduction of energy barriers (the more negative material) in the transport pathways to the current collector. It has been found that the coating may have a number of different effects. For example Nb_2O_5 coat, whose conduction band potential is 100 mV negative than that of the TiO_2 core particles, primarily forms of a “kinetic barrier” for recombination.[84] On another hand $SrTiO_3$, that should form a 200 mV barrier on TiO_2, produces a shift of the conduction band of the core TiO_2 as a consequence of surface dipole generated at the $TiO_2/SrTiO_3$ interface, and consequently the open circuit photovoltage increases, while the short circuit photocurrent decreases.[86] It has been suggested that barrier coatings with high points of zero charge (basic coatings) are most effective for the retardation of the recombination dynamics.[74] Impedance spectroscopy of Al_2O_3-coated TiO_2 films showed that the thin alumina layer mainly passivates the surface states in the TiO_2 and therefore reduces the recombination rate.[90] Transient photovoltage (PV) spectroscopy results[91] also to show that ultrathin alumina layers prevent the formation of defects at the TiO_2 surface.[91] It was found that the PV signal increases already at photon energies above 1 eV for the uncoated TiO_2, indicating strong absorption at defect states, while the TiO_2/Al_2O_3 films show PV signal only above 3.1 eV, the bandgap of TiO_2. The authors suggested[91] that the alumina stabilizes the chemical potential of oxygen at the surface. Recently Zaban and coworkers[92] analysed a new type of high surface area TiO_2 electrode for DSCs, consisting of a transparent conductive nanoporous matrix that is coated with a thin layer of TiO_2. This design ensures several nanometer distance between the TiO_2-electrolyte interface and the current collector throughout the nanoporous electrode, in contrast to several microns associated with the standard electrode. However it was found that the photovoltaic performance of TiO_2 coating thinner than 6 nm is rather inefficient.[92]

The short-circuit photocurrent in a DSC is a central device parameter that depends mainly on two factors: light harvesting/electron injection, and electron transport, provided that electrolyte processes are not limiting the DSC operation.

Strategies have been developed for improving the DSC conversion efficiencies by increasing the light harvesting, especially in the low energy (red and near-IR) region of the solar spectrum. Dye molecules with high red absorbance have poor injection yields because of the low lying excited state (LUMO). Increasing the thickness of the film beyond 10 μm in order to increase the absorbance in the red results in an increase in the electron transport length and the recombination rate, thereby decreasing the photocurrent. Furthermore, conventional nanocrystalline TiO_2 films formed by 10-30 nm nanoparticles are poor light-scatterers. The addition of 4-5 μm thick light scattering layers of 400 nm TiO_2 particles to the conventional nanocrystalline layer enhances light harvesting in the red and near-IR spectral region by enhancing the scattering of light.[93-95] TiO_2 photonic crystals and disordered scattering titania inverse opal structures have also been exploited to increase the light conversion efficiency of DSC, improving the conversion efficiency in the spectral range of 600-800 nm.[96,97] A theoretical analysis shows improved photocurrent efficiency due to the mirror behaviour of the colloidal superlattice.[98]

Electron transport in DSC is driven mainly by diffusion, due to the effective electrolyte shielding of space charge. Detailed information on the physical parameters related to transport in DSCs has been obtained using small perturbation techniques at a fixed steady state such as IMPS[38,39] and impedance spectroscopy.[26,31,90] It was found that both the effective electron diffusivity, D_n, and the effective electron lifetime, τ_n,[75,99] that are measured, become a function of the steady state.[34,38,43,67,75,100-104] This has usually been considered an effect of the distribution of bandgap electronic states that influence the time constants. Variations of both, diffusion coefficient and lifetime, were attributed to the statistics of electrons in the material, which deviates from dilution, as described by thermodynamic factors.[105]

The simplest approach to take trapping into account is the classical multiple trapping (MT) framework[106-109] which has been applied to DSC by a number of authors.[34,38,110-112] In this approach, transport through extended states is slowed down by trapping-detrapping events, while direct hopping between localized states is neglected. Electronic states are composed of a transport level (usually identified with the lower edge of the conduction band) at the energy level E_c, with a diffusion coefficient D_0, and a density of localized states $g(E)$ distributed in the bandgap. The total electron density is $n = n_c + n_L$, i.e. the sum of electron densities in conduction band (with an effective DOS N_c) and localized states. The mobility decreases rapidly below the level E_c defining the transport states, so that the motion of a bound electron is limited by the rate of thermal excitations to $E \geq E_c$. The varying D_n in this model was recognized as a chemical diffusion coefficient[112,113] that is given by

$$D_n = \left(\frac{\partial n_c}{\partial n_L} \right) D_0 \tag{13}$$

The prefactor in Eq. (13) is the relationship of free to trapped number of electrons for a small variation of the Fermi level. This prefactor describes the delay of response of the chemical diffusion coefficient, with respect to the free electrons diffusion coefficient, by the trapping and detrapping process.[105,114] The calculation of the chemical diffusion coefficient for an exponential distribution gives an exponential dependence on the Fermi-level position as follows[112,113]

$$D_n = \frac{N_c T_0}{N_L T} \exp\left[(E_{Fn} - E_c) \left(\frac{1}{k_B T} - \frac{1}{k_B T_0} \right) \right] D_0 \tag{14}$$

The functional dependence in Eq. (14) is a consequence of the exponential variation of the time constant for detrapping when the Fermi level scans the bandgap in Fig. 11.

Fig. 13. Parameters resulting from fit of experimental impedance spectroscopy spectra of three DSCs at different bias potentials in the dark. The electrolyte compositon in the reference cell is 0.5M LiI, 0.05M I_2, 0.5 1-methylbenzimidazole (MBI) in 3-methoxypropionitrile (3-MPN). The second cell has 0.5M NaI instead of LiI, and the third cell has no MBI. (a) Capacitance of the cell without the contribution of the platinum counterelectrode capacitance. (b) Chemical diffusion coefficient of electrons. The lines are fits to the multiple trapping/exponential distribution (characteristic temperature T_0) model, and the parameters resulting from fits are indicated. T is the actual temperature of the cell, assumed 300 K, T' is the effective temperature obtained from the slope of the plots as indicated. Adapted from Sol. Energy Mater. Sol. Cells **87**, F. Fabregat-Santiago, J. Bisquert, G. Garcia-Belmonte, G. Boschloo and A. Hagfeldt, 117, "Impedance spectroscopy study of the influence of electrolyte conditions in parameters of transport and recombination in dye-sensitized solar cells", Copyright 2005, with permission from Elsevier.

In order to illustrate the connection between the DOS and the measured electron diffusion coefficient, we show in Fig. 13 the chemical capacitance, C_μ and chemical diffusion coeficient D_n, obtained by impedance spectroscopy for three DSCs containing different species in the electrolyte.[31] The two elements C_μ and D_n show exponential dependencies in the potential, in agreement with Eqs. (9), (10) and (14). Furthermore for the different cells these parameters display a global shift in the voltage axis for the different surface treatments, which demonstrates the global displacement of the TiO_2 energy levels in the energy axis, caused by the absorption of the indicated species, in the same way as in Fig. 12, above. Fitting the capacitance of the reference cell, containing LiI electrolyte, in Fig. 13a, in the intermediate domain where the chemical capacitance is observed separately from other capacitive contributions, it is obtained $k_B T_0 = 62\,\mathrm{mV}$ corresponding to $T/T_0 = 0.42$ at $T = 300\,\mathrm{K}$. This predicts an exponent $k_B T/(1-T/T_0) = 44\,\mathrm{mV}$ for the voltage-dependence of the chemical diffusion coefficient, and this in fact is the value obtained in Fig. 13b. Therefore the MT gives a consistent description of the observed features of electron transport and accumulation in anatase-TiO_2 DSC. However the free electron displacement in the conduction band/transport level, predicted by the model when the Fermi level raises to fill most of the traps, has not been separately observed, possibly due to the difficulty of measuring at such negative potential by the bandshift inducced by electron charging.

The measurement of the electron lifetime consists on determining the time for the system to recover equilibrium under a small perturbation of the steady state, by removal of the excess carriers by recombination.[99] In DSC, the lifetime can be determined by monitoring directly the variation of the position of the Fermi level with time (open-circuit photovoltage decay technique).[75,99] Assuming a process of trapping-detrapping in the bulk of a nanoparticle, and injection to the electrolyte from a single (conduction band) energy level, the time constant for the decay takes the form[99]

$$\tau_n = \left(\frac{\partial n_L}{\partial n_c} \right) \tau_{n0} \tag{15}$$

where τ_{n0} is the lifetime of the electron in the (conduction band) injection level. Equation (15) predicts an exponential dependence of the lifetime with the Fermi level that is indeed found in many reports.[38,39,115] It is observed in Eqs. (13) and (15) that the factors $(\partial n_L / \partial n_c)$ in D_n and τ_n, compensate when forming the diffusion length from measured quantities. The result is a constant

$$L_n = \sqrt{D_n \tau_n} = \sqrt{D_0 \tau_{n0}} \quad (16)$$

The meaning of the compensation is clear when we note that the origin of the factor $(\partial n_L / \partial n_c)$ lies in carrier equilibration in the energy space, both for chemical diffusion coefficient in MT (D_n), and for measured lifetime (τ_n). Peter and co-workers[38,115] and also Nakade et al.[43] have reported for DSCs the compensating behaviour indicated in Eq. (16).

Measurements of the electron lifetime over a more extended voltage domain, indicated in Fig. 14, show a more complex picture. In the important domain of the solar cell operation between 0.6 and 0.8 V, the lifetime depends exponentially on the potential, in agreement with the previously mentioned results. However at lower potentials there is a strong variation, and at higher potentials, the lifetime becomes constant. This behaviour indicates a combination of several processes that govern electron recombination in DSC.[75-77]

Fig. 14. Electron lifetime determined from the decay of the cell potential in a DSC following application of a negative bias (> -1.2 V) in the dark. The line corresponds to the fit to a model that uses the quasi-static approximation for trapping in the bulk and a combination of charge transfer processes through conduction band and surface states. Adapted with permission from J. Bisquert, A. Zaban, M. Greenshtein and I. Mora-Seró, J. Am. Chem. Soc. **126**, 13550. Copyright 2004 American Chemical Society.

Besides the energy disorder that has been already emphasized for describing the diffusion coefficient, the extent of geometry disorder has been recognized as an important property of the nanocrystalline TiO_2 electrodes in DSC, due to the influence on long-range paths for electron transport.[116,117] Geometrical disorder may become rather significant for open structures of the nanoparticulate network, owing to the existence of highly branched nanoparticle structures that influence electron transport dynamics. For example for compact TiO_2 films (40% porosity) used in DSC, the average coordination number is about 6.6, whereas for open-structured films (80% porosity), the average number of particle interconnections is as low as 2.8.[116] Therefore, when increasing the porosity the fraction of terminating particles (dead ends) in the TiO_2 film increases markedly, and this has the effect of increasing the average number of particles visited by electrons by 10-fold.[117] Figure 15 shows the reported[44] evolution of the diffusion coefficient of electrons in nanostructured TiO_2, as a function of the excess porosity above the critical value for transport. Samples of different porosity are achieved by consecutive pressing the TiO_2 film, from 7 to 4 μm thickness. Using this method of changing the film thickness the energy distribution and trapping factors are not significantly dependent on sample porosity. Therefore the results show a change of the diffusion coefficient that is due to the geometrical effect of the coordination between nanoparticles. The power law behaviour with porosity obtained in Fig. 15 is related to electron diffusion along the percolation cluster in the nanoparticulate network as first suggested by Jao van de Lagemaat and co-workers.[116,117]

Fig. 15. Plot of the effective (chemical) diffusion coefficient of electrons, obtained from transient photocurrents, as a function of the porosity of TiO_2 layers. The critical porosity was set to 0.76. Reused with permission from Th. Dittrich, A. Ofir, S. Tirosh, L. Grinis, and A. Zaban, Appl. Phys. Lett., **88**, 182110. Copyright 2006, American Institute of Physics.

Microscopic simulation using Monte-Carlo methods based on Continuous Time Random Walk (CTRW) model have been applied to provide a detailed description of electron trapping dynamics in DSC.[116-120] Simulations have described the results of fast optical pump-probe

experiments that monitor the decay of the photoinduced dye cation excited by a laser pulse.[121-123] Recently[124] CTRW methods have provided valuable insights into the short range diffusion and charge separation in dye-sensitized nanoscale TiO_2 layers measured by surface photovoltage transients.[125,126]

Hole or ion conduction in the medium filling the pores can be realized in different configurations. The 11% conversion efficiency has been reached with the N3 dye, and a liquid electrolyte with iodine/iodide redox couple with a film thickness of over 15μm. However the longterm containment at elevated temperatures of the volatile solvent mixture employed still remains a major challenge. Therefore there has been extensive quest for a solid or quasi-solid medium for replacing the volatile electrolyte while maintaining good performance of the DSC. A number of options for the ionic/hole transport material have been investigated:[127]

- Inorganic p-type semiconductors.[128]
- Organic hole-transport materials (HTM) such as spiro-OMeTAD (2,2'7,7'-tetrakis(N,N-di-p-methoxyphenyl-amine)-9,9'-spiro-bifluorene).[71,104,129,130]
- Polymer electrolytes.
- Ionic liquid conductors.[19,131-133]

It appears that the I_3^-/I^- couple is unique in providing the strong kinetic asymmetry of recombination/regeneration reactions that gives so far the highest efficieny in DSC.[57] Organic hole conductors generally exhibit lower differential kinetics than I_3^-/I^- couple and therefore provide a poorer performance of the solar cell. Room temperature ionic liquids (RTIL) are solvent free redox systems with high stability and negligible vapor pressure, that are considered a key element for practical applications of the DSC.[134,135] The very high density of ions present in these RTILs appears to facilitate the effective screening of the electric charges that are produced under illumination in the mesoporous films.[127] DSC using RTIL have shown practical efficiencies in the range 6-7% and an improved stability at high temperatures. The limitation of the slow diffusion of iodide redox species in the viscous RTIL is currently being addressed by the development of novel sensitizers with an increased optical cross section allowing thinner TiO_2 films to be employed.[95]

Complete models of the DSC have been developed based on porous battery theory,[136,137] considering mass transport in the electrolyte,[131,138-142] higher-order recombination mechanisms[143] and the porosity effect.[144] These methods allow the simulation of the photovoltaic performance of the DSC but involve a multitude of effects and complex calculation. While V_{oc} and I_{sc} can be separately related to basic processes of the DSC, as already discussed, the understanding of the diode characteristics, i.e. the FF, which is critical for device performance, has so far not been described in a simplified framework.

All-solid solar cells based on nanostructured or highly-structured metal oxide materials have been developed in different configurations,[9,145-148] either with a thin light-absorber layer, or with an absorber/hole transport material embedded in the nanostructured metal oxide. A nanocomposite solar cell, based on interpenetrating networks of TiO_2 and $CuInS_2$, has provided the highest energy conversion efficiency, of around 5%, of this type of solar cells.[149]

5.-Nanostructured photoelectrochemical and electrochemical devices based on metal-oxide nanoparticles

The photocatalytic splitting of water into hydrogen and oxygen using solar light is a potentially clean and renewable source for hydrogen fuel. There has been extensive investigation into metal-oxide semiconductors such as TiO_2, WO_3, and Fe_2O_3, which can be used as photoanodes.[12,13,150] The extension of the absorption of TiO_2 to the visible spectrum of the solar spectrum, by doping with carbon, nitrogen or sulfur,[151,152] has stimulated great interest, but the use of such materials has provided low conversion efficiencies so far. Nanoparticulate WO_3 electrodes exhibit larger photocurrents under solar illumination,[12,150] due to the band-gap energy of 2.5 eV that extends the photoresponse of WO_3 electrode into the blue part of the visible spectrum up to 500 nm. The photoelectrochemical behaviour of nanostructured TiO_2 and WO_3 electrodes, concerning the photooxidation of organic compounds in water, has been studied in a

number of works.[153-159] The company Hydrogen Solar Ltd, UK, is trying to implement a tandem cell for the cleavage of water to hydrogen and oxygen by visible light based on work by M. Grätzel and J. Augustynski. The photoactive material in the top cell is a semiconducting oxide that absorbs the blue and green part of the solar emission spectrum and generates oxygen and protons from water with the energy collected. The not absorbed yellow and red light transmits the top cell and enters a DSC.[157]

Electrochromism is a reversible process inducing optical transitions in a material via an electrochemical reaction.[160] Electrochromism is of importance for applications in information displays with optical memory, smart windows, and anti-dazzling rear view mirrors for cars with variable reflectance. The most studied electrochromic material is WO_3, which turns from transparent to dark blue upon insertion of H, Li and other guest atoms. Smart windows with switchable glazing allow dynamic control of solar energy gain, adapting the window optical properties to changing environmental conditions. Especially in temperate zone climates, solar radiation in summer conditions imposes an unwanted heat load on buildings, while passive heating by solar radiation is welcome in winter.[161] One of the limitations of WO_3 intercalation films for implementation of glass window with variable optical properties in a large scale, is the requirement of external power sources to change the transmittance. To remove this limitation, self-powered smart windows combining a DSC with an WO_3 electrochromic layer counterelectrode have been suggested.[2] A switchable photoelectrochromic device has been realized consisting on a dye-covered nanoporous TiO_2 layer, which is situated on a nanoporous WO_3 electrochromic layer.[162-164] All the layers can be kept quite thin, so that they are transparent. The transmittance of the device decreases when illuminated and can be increased under short-circuit conditions. Therefore, no external voltage source is needed to colour/bleach the photoelectrochromic device.

Another approach to electrochromic devices that has proved sucessful for electrical displays applications was originally developed by M. Grätzel and D. Fitzmaurice.[10] It consists of nanocrystalline TiO_2 films derivatized with a redox active molecule, such as a viologen endowed with an anchoring group to attach it firmly to the TiO_2 surface. Viologens (e.g. 1,1'-disubstituited 4,4'-bipyridinium dications) work as redox chromophores. The first reduction of the viologen dication is highly reversible and leads to the formation of the intensely deep blue coloured radical cation. The devices present rapid switching between the bleached and coloured states, high contrast ratios and good cycling stability,[27,165-169] due to the amplification of the optical phenomena by the high surface area of the nanocrystalline support, and fast interfacial electron transfer between the nanocrystalline oxide and the adsorbed modifier. Photoelectrochemical studies have shown[27] that the electronic charging of the semiconductor nanostructure is the key factor mediating between the electrode potential and colouration of the molecular monolayers anchored on the semiconductor surface. Displays based in this technology are close to commercialization by the company NTera, that has announced in 2006 the successfull production of working prototypes featuring the world's highest resolution naturally reflective electronic displays, and plans to produce a high-contrast, monochromatic display that can replace the simple liquid crystal displays used in clocks, thermostats and many other devices.

The optical and visible-sensitizing functions of molecular layers absorbed onto nanocrystalline metal oxides have been widely exploited in DSC and electrochromics, as commented above. Recently a new approach has been taken towards electric and electro-optic devices formed by molecular functionalized mesoscopic oxides, such as sensors and switchable molecular electronics, in which the molecular layer adsorbed in the surface, serves instead as an electron or hole transport relay.[170-174] It was shown that the molecular layer can be charged from the conductive ubstrate either with electrons or holes, depending on the applied bias potential.[171,172] Figure 16 shows impedance spectroscpy results of mesoscopic Al_2O_3 and TiO_2 networks, covered with a monolayer of Ru-complex *cis*-RuLL'$(NCS)_2$ (L=2,2'-bipyridyl-4,4'-dicarboxylic acid, L'=4,4'-dinonyl-2,2'-bipyridyl) (Z907).[30] The results display the behaviour of the model of Fig. 5, at potentials in which injection of carriers in the respective semiconductor networks is forbidden. These results therefore show the injection, transport and accumulation of

electrons and holes in the molecular layers covering the surface of the mesoscopic oxides.[30]

Fig. 16. Experimental impedance plots of Z907-derivatized mesoscopic TiO_2 and Al_2O_3. Reprinted with permission from J. Bisquert, M. Grätzel, Q. Wang and F. Fabregat-Santiago, J. Phys. Chem. B **110**, 11284. Copyright 2006 American Chemical Society.

TiO_2 is biocompatible and combines selectively with some groups of biomolecules. Nanocrystalline TiO_2 has been employed for the immobilization of biomolecules,[4,69,175] both for studying protein electrochemistry, and for developing electrochemical biosensors, i.e., analytical devices consisting of a biological recognition element attached to the nanostructured TiO_2 that serves as a transduction element, relating the concentration of an analyte to a mesurable response.[176]

The conductivity of nanostructured TiO_2 in the gas phase[177-180] and as a function of ambient humidity has been described.[181] The group of J. Augustynski has developed nanoparticles of semiconducting metallic oxides employed in gas sensors able to detect nitrogen oxides, carbon monoxide and hydrocarbons. These nanocrystalline oxides (not disclosed, but apparently comprising WO_3 nanoparticles) are used by the Company MicroChemical Systems for manufacturing gas sensors for automotive industry. The two types of micro-sensors measure changes in the electrical resistance of nanocrystalline films induced by road gas pollutants, resulting in improved sensitivity and response time of the micro-sensors fabricated by MicroChemical Systems, which has already delivered such micro-sensors in large quantities to car makers.

The use of nano-sized positive or negative electrode materials (*vs.* Li) for Li batteries[14,182] offers attractive electrochemical characteristics over classical bulk materials, including very short diffusion length, low charge transfer resistance due to the high surface area of the active mass[182] and a better accommodation of the materials strains associated with the lithium insertion/extraction. The active material/electrolyte interface can be improved by acting on the current collector surface. Nano-architectured current collectors offer higher contact area than conventional 2D-substrate. As a result, for an equivalent thickness, the amount of active material is much higher on a nano-structured current collector. However, an adverse effect in primary nanoparticles is the possibility of increasing side reactions with the electrolyte, while the Li-reaction may be enhanced.[183] TiO_2 nanotubes or nanowires have shown excellent Li-intercalation charge capacity and cyclability.[184,185] The Li^+ intercalation renders the nanowires simultaneously electronically and ionically conducting.[185] As in other devices commented earlier on, the electrolyte is a crucial element in Li-batteries. It has been found that the addition of nanoparticle fillers, such as Al_2O_3 or TiO_2, increases several fold the conductivity of polymer electrolytes at 60–80ºC, and prevents crystallization at room temperature.[186]

Supercapacitors are high-power density devices that can be coupled with batteries to provide peak power and can replace batteries for memory back-up. High-surface-area carbon-based materials are widely used for electrochemical double layer supercapacitors. A nanostructured $Li_4Ti_5O_{12}$ has been developed as a negative electrode material suitable for use with activated carbon positive electrodes.[187,188] The combined effect of a high output voltage and an anode of greater specific capacity results in higher energy densities than carbon/carbon supercapacitors, while maintaining a high power density and robustness.

6.-Ordered nanoparticulate structures

Quantum dots are nanocrystals of size roughly between 1 and 10 nm. In these crystals the electron wave functions are delocalized in the limited space of the nanocrystal, and the electronic orbital has the same symmetry as in a conventional atom. The strong quantum confinement implies that insulating nanocrystals have a set of discrete atom-like valence and conduction energy levels. Their separation as well as the optical gap between the lowest conduction level and the highest valence level increases as the nanocrystal size decreases. Accordingly, electronic and electrooptic properties of quantum dots can be tailored by the

dimensions.

Colloidal nanocrystals can be considered as building blocks for larger arquitectures. Nanocrystals with a narrow size dispersion can be assembled into two-dimensional or three dimensional ordered arrays, which are termed nanocrystal superlattices, nanocrystal solids or quantum dot solids. The particles are characterized by an inorganic core and stabilized by an organic surfactant, and both the core and the surfactant have a role in determining the superlattice crystallographic symmetry. Since both the preparation of nanocrystals and the ordered assemblies is versatile, there is currently great interest in the investigation of the properties of the quantum dot solids.[15,16,189]

The collective properties of electrons injected in a superlattice depend on individual electronic levels for a quantum dot, on the degree of electronic coupling between the dots, and also on Coulomb interactions, both for multiple electrons in a quantum dot and in neighbour dots.[16] Assemblies of quantum dots deposited on a conducting substrate, and filled with an ionic medium, allow the injection of a single kind of carrier in the superlattice. The Coulomb energy of electrons in a dot is considerably reduced by screening with electrolyte ions, as commented in connection to Figs. 1 and 2. The energy for addition of electrons to a quantum dot contains several contributions:[190,191] the self-energy of the electron interacting with its image charge at the surface of the particle,[192] the electrostatic interactions, which are screened by the external medium, and the exchange energy. Characteristic capacitance spectra showing consecutive charging of different discrete energy levels, have been reported for assemblies of CdSe[193,194] and ZnO colloids.[195]

An ordered array of quantum dots could give rise to long range coherent transport in delocalized bands, provided that sufficient electronic coupling exists between the same orbitals in neighbor dots. However, there are several factors that lead to localization of carriers in the quantum dots.[189] Colloidal nanoparticles prepared by wet chemical methods fluctuate in size. Since the electronic response of an individual particle is determined by its size, there is some inherent disorder in an array of quantum dots, that produces a dispersion of the energy levels.[189] Dispersion of energy levels can be also caused by a fluctuation of chemical composition (e. g. electronic surface states). The difference between energy levels in different quantum dots makes tunneling of electrons between quantum dots more difficult. Moreover such dispersion leads to the random scattering of electronic waves. Thus dispersion of quantum dots sizes and fluctuation of the chemical composition, produce Anderson localization. Disorder in the spatial distribution of quantum dots also contributes to localization.[196] The Coulomb repulsion between two electrons (holes) sitting on the same quantum dot introduces an energy gap between occupied and empty states (Hubbard insulator). A number of characteristic phenomena for transport in disordered semiconductors have been reported in arrays of quantum dots, such as metal-insulator transitions [15,197] and Mott-like conduction gaps[62,196], the variable range hopping (VRH) transport,[198] temperature scaling in current-potential curves[199] and percolation thresholds depending on disorder.[200] Experimental studies of arrays of monodisperse ZnO quantum dots, charge-compensated in electrolyte solution, have been reported.[195,201,202] The influence of size dispersion over collective transport properties in these systems has been examined theoretically.[203]

Ordered mesoporous materials with periodicity on an optical length scale can lead to materials that exhibit a full photonic band gap, i.e., a wavelength band in which photon propagation is forbidden.[204] These photonic materials can be integrated into substrates of technological interest[205] and can be used in applications in which the manipulation of the flow of visible and near-IR light is required, as commented before for improving light-harvesting in DSC. TiO_2 is an attractive material for the fabrication of photonic bandgap materials, especially the inverse opal, air spheres in TiO_2 matrix, due to the high refractive index and good transparency of TiO_2 for the visible light. Inverse titania opal photonic crystals have shown effective to control the spontaneous emission from semiconductor quantum dots embedded in the photonic crystal.[206] In these experiments the crystal lattice parameter could be used to enhance of delay the decay rates of light emission from the quantum dots. Dye-sensitized and solid-state solar cells have been fabricated on microporous titania inverse opal structures.[207,208] The electrochemical behaviour of these structures under Li intercalation was investigated.[209]

7. Nanowires and nanotubes

Nanowires and nanotubes are drawing a tremendous attention due to their potential applications in various nanoscale devices. Among the oxide materials, those having a bulk crystalline structure in form of layers or ribbons can be more easily induced to grow in the form of rods or tubes with high aspect ratio and nanometric dimensions.[17]

ZnO nanostructures such as nanowires, nanotubes, and nanorings have been grown successfully via a variety of methods including chemical vapor deposition, thermal evaporation, and electrodeposition.[210] Zinc oxide is a nontoxic *n*-type semiconductor that has favorable band energies for forming heterojunctions with hole-conducting polymers and can be grown as nanorod arrays with the appropriate dimensions for efficient nanorod-hole conductor devices. Vertically aligned ZnO nanorods, formed by electrodeposition on a transparent conducting oxide have attracted much attention for applications in UV-optoelectronic devices such as light emitting diodes.[11] Due to its near-cylindrical geometry and large refractive index, ZnO nanowire/nanorod is a natural candidate for optical waveguide, and for optical resonant cavities with facilitate lasing in well-aligned ZnO nanowires.[211]

With respect to solar cells based on nanoparticulate metal oxides, nanowire structures have the advantage of providing long and uninterrupted paths for electron transport while maintaing a high area density.[212-214] ZnO nanowires have been used to form high heterojunction area solar cells,[9,147,212,215] in particular CdSe-sensitized CuSCN/nanowire ZnO heterojunctions have shown an encouraging photovoltaic performance.[9] There has been recent progress in obtaining highly ordered transparent TiO_2 nanotube arrays for DSC with high electron lifetimes and excellent pathways for electron percolation.[216] Carbon-doped TiO_2 ($TiO_{2-x}C_x$) nanotube arrays have also shown high photocurrent densities and more efficient water splitting under visible-light illumination than TiO_2 nanoparticles.[217]

Recent literature results[218-220] have demonstrated that V oxides, such as V_2O_5, can be produced in form of nanowires by means of different techniques, i.e. by hydrothermal, sol-gel, sol electrophoretic or sol electrochemical deposition. V_2O_5 nanowires have many intrinsic merits, such as an uniform geometric cross-section of 1.5 nm × 10 nm and several micrometer length, which are important in nanofunctional materials. The heterojunction of V_2O_5 nanowires with carbon nanotube, field effect transistor and actuators as artificial muscles have been demonstrated as feasible electronic components.[221] The fibers show a double layer structure, with each layer consisting of two V_2O_5 sheets. A V_2O_5 fiber is composed of only four atomic layers of vanadium, which therefore represents a wire with a thickness of molecular dimension. The conductivity of one individual V_2O_5 fiber was estimated to be ~0.5 S/cm at room temperature.[220] The electrochemical Li-intercalation behaviour of nanoscale V_2O_5 was found to depend markedly on the morphology and defect structure.[222]

Nanowires and nanotubes are also encouraging structures for chemical and biological sensors in which detection can be monitored electrically and/or optically. For example when helium gas is absorbed physically into the interlayer or on the surface of soft V_2O_5 nanowires, it is possible to detect the helium gas from the variation of conductance through the nanowires.[223] With molecular receptors or a selective membrane for the analyte of interest, the binding of a charged species to the surface of a nanowire or nanotube can lead to depletion or accumulation of carriers in the “bulk” of the nanometer diameter structure and increase sensitivity to the point that single-molecule detection is possible.[224]

Acknowledgments

The author is grateful to Jan Augustynski, Franco Decker, Michael Grätzel, Ian S. Plumb, Daniel Vanmaekelbergh and Arie Zaban, for their useful comments on nanostructured devices. The work was supported by Ministerio de Educación y Ciencia of Spain under project MAT2004-05168.

References

[1] O' Regan B,Grätzel M, *Nature*, 353, 737 (1991).
[2] Bechinger C, Ferrer S, Zaban A, Sprague J,Gregg B A, *Nature*, 383, 608 (1996).
[3] Cinnsealach R, Boschloo G, Rao S N,Fitzmaurice D, *Sol. Energy Mater. Sol. Cells*, 57, 107 (1999).
[4] Topoglidis E, Palomares E, Astuti Y, Green A, Campbell C J,Durrant J R, *Eletroanalysis*, 17, 1035 (2005).
[5] Grätzel M, *Nature*, 414, 338 (2001).
[6] Grätzel M, *J. Photochem. Photobiol. A: Chem.*, 164, 3 (2004).
[7] Bisquert J, Cahen D, Rühle S, Hodes G,Zaban A, *J. Phys. Chem. B*, 108, 8106 (2004).
[8] Hagfeldt A,Grätzel M, *Chem. Rev.*, 95, 49 (1995).
[9] Lévy-Clément C, Tena-Zaera R, Ryan M A, Katty A,Hodes G, *Adv. Mat.*, 17, 1512 (2005).
[10] Grätzel M, *Nature*, 409, 575 (2001).
[11] Könenkamp R, Word R C,Godinez M, *Nano Lett.*, 5, 2005 (2005).
[12] Wang H, Lindgren T, He J, Hagfeldt A,Lindquist S-E, *J. Phys. Chem. B*, 104, 5686 (2000).
[13] Jorand-Sartoretti C, Alexander B D, Solarska R, Rutkowska I A, Augustynski J,Cerny R, *J. Phys. Chem. B*, 109, 13685 (2005).
[14] Aricò A S, Bruce P, Scrosati B, Tarascon J M,van Schalkwijk W, *Nat. Mat.*, 4, 366 (2005).
[15] Collier C P, Vossmeyer T,Heath J R, *Ann. Rev. Phys. Chem.*, 49, 371 (1998).
[16] Vanmaekelbergh D,Liljerorth P, *Chem. Soc. Rev.*, 34, 299 (2005).
[17] Patzke G, Krumeich F,Nesper R, *Angew. Chem. Int. Ed.*, 41, 2446 (2002).
[18] Huang S Y, Kavan L, Exnar I,Grätzel M, *J. Electrochem. Soc.*, 142, L142 (1995).
[19] Wang P, Zakeeruddin S M, Exnar I,Grätzel M, *Chem. Commun.*, 2972 (2002).
[20] Zaban A, Micic O I, Gregg B A,Nozik A J, *Langmuir*, 14, 3153 (1998).
[21] Bisquert J, Garcia-Belmonte G,Fabregat Santiago F, *J. Solid State Electrochem.*, 3, 337 (1999).
[22] Winter M,Brodd R J, *Chem. Rev.*, 104, 4245 (2004).
[23] Bisquert J, Garcia-Belmonte G, Fabregat-Santiago F, Ferriols N S, Bogdanoff P,Pereira E C, *J. Phys. Chem. B*, 104, 2287 (2000).
[24] Bisquert J, *J. Phys. Chem. B*, 106, 325 (2002).
[25] Pitarch A, Garcia-Belmonte G, Mora-Seró I,Bisquert J, *Phys. Chem. Chem. Phys.*, 6, 2983 (2004).
[26] Fabregat-Santiago F, Garcia-Belmonte G, Bisquert J, Zaban A,Salvador P, *J. Phys. Chem. B*, 106, 334 (2002).
[27] García-Cañadas J, Fabregat-Santiago F, Kapla J, Bisquert J, Garcia-Belmonte G, Mora-Seró I,Edwards M O M, *Electrochim. Acta*, 49, 745 (2004).
[28] Gregg B A, *Coord. Chem. Rev.*, 248, 1215 (2004).
[29] Grätzel M, *Current Applied Physics*, in press (2006).
[30] Bisquert J, Grätzel M, Wang Q,Fabregat-Santiago F, *J. Phys. Chem. B*, 110, 11284 (2006).
[31] Fabregat-Santiago F, Bisquert J, Garcia-Belmonte G, Boschloo G,Hagfeldt A, *Sol. Energy Mater. Sol. Cells*, 87, 117 (2005).
[32] Wang Q, Moser J-E,Grätzel M, *J. Phys. Chem. B*, 109, 14945 (2005).
[33] Hoshikawa T, Kikuchi R,Eguchi K, *J. Electroanal. Chem.*, 588, 59 (2006).
[34] de Jongh P E,Vanmaekelbergh D, *Phys. Rev. Lett.*, 77, 3427 (1996).
[35] Vanmaekelbergh D, Iranzo Marín F,van de Lagemaat J, *Ber. Bunsenges. Phys. Chem.*, 100, 616 (1996).
[36] Vanmaekelbergh D,de Jongh P E, *Phys. Rev. B*, 61, 4699 (2000).
[37] Dloczik L, Ileperuma O, Lauerman I, Peter L M, Ponomarev E A, Redmond G, Shaw N J,Uhlendorf I, *J. Phys. Chem. B*, 101, 10281 (1997).
[38] Fisher A C, Peter L M, Ponomarev E A, Walker A B,Wijayantha K G U, *J. Phys. Chem. B*, 104, 949 (2000).
[39] Schlichthörl G, Huang S Y, Sprague J,Frank A J, *J. Phys. Chem. B*, 101, 8141 (1997).
[40] Solbrand A, Lindström H, Rensmo H, Hagfeldt A, Lindquist S E,Södergren S, *J. Phys. Chem. B*, 101, 2514 (1997).

[41] Solbrand A, Henningsson A, Sodergren S, Lindstrom H, Hagfeldt A,Lindquist S-E, *J. Phys. Chem. B*, 103, 1078 (1999).
[42] Noack V, Weller H,Eychmüller A, *J. Phys. Chem. B*, (2002).
[43] Nakade S, Saito Y, Kubo W, Kitamura T, Wada Y,Yanagida S, *Electrochem. Commun.*, 5, 804 (2003).
[44] Dittrich T, Ofir A, Tirosh S, Grinis L,Zaban A, *Applied Physics Letters*, 88, 182110 (2006).
[45] Zhang Z, Zakeeruddin S M, O'Regan B C, Humphry-Baker R,Grätzel M, *J. Phys. Chem. B*, 109, 21818 (2005).
[46] Kern R, Sastrawan R, Ferber J, Stangl R,Luther J, *Electrochim. Acta*, 47, 4213 (2002).
[47] Mora-Seró I, Bisquert J, Fabregat-Santiago F, Garcia-Belmonte G, Zoppi G, Durose K, Proskuryakov Y, Oja I, Belaidi A, Dittrich T, Tena-Zaera R, Katty A, Lévy-Clement C, Barrioz V,Irvine S J C, *Nano Letters*, in press (2006).
[48] Fabregat-Santiago F *PhD Thesis* Universitat Jaume I: Castelló (2001).
[49] de Levie R, in *Adv. Electrochem. Electrochem. Eng.*; *Vol. 6*, edited by Delahay P Interscience, New York (1967), p. 329.
[50] Raistrick I D, *Electrochim. Acta*, 35, 1579 (1990).
[51] Pajkossy T, *J. Electroanal. Chem.*, 364, 111 (1994).
[52] Pajkossy T, Wandlowski T,Kolb D M J, *J. Electroanal. Chem.*, 414, 209 (1996).
[53] Kötz R,Carlen M, *Electrochim. Acta*, 45, 2483 (2000).
[54] Lampert M A,Mark P *Current Injection in Solids* Academic: New York (1970).
[55] Blom P W M,Vissenberg M C J M, *Mat. Sci. Eng. R*, 27, 53 (2000).
[56] Mihailetchi V D, Wildeman J,Blom P W M, *Phys. Rev. Lett.*, 94, 126602 (2005).
[57] Peter L M, *J. Electroanal. Chem.*, in press (2006).
[58] Mora-Seró I,Bisquert J, *Sol. Energy Mater. Sol. Cells*, 85, 51 (2005).
[59] Bisquert J, *Phys. Chem. Chem. Phys.*, 2, 4185 (2000).
[60] Abayev I, Zaban A, Fabregat-Santiago F,Bisquert J, *Phys. Stat. Sol. (a)*, 196, R4 (2003).
[61] Meulenkamp E A, *J. Phys. Chem. B*, 103, 7831 (1999).
[62] Roest A L, Kelly J J,Vanmaekelbergh D, *Appl. Phys. Lett.*, 83, 5530 (2003).
[63] Agrell H G, Boschloo G,Hagfeldt A, *J. Phys. Chem. B*, 108, 12388 (2004).
[64] Bisquert J, *Phys. Chem. Chem. Phys.*, 5, 5360 (2003).
[65] Kytin V G, Bisquert J, Abayev I,Zaban A, *Phys. Rev. B*, 70, 193304 (2004).
[66] Fabregat-Santiago F, Mora-Seró I, Garcia-Belmonte G,Bisquert J, *J. Phys. Chem. B*, 107, 758 (2003).
[67] Niinobe D, Makari Y, Kitamura T, Wada Y,Yanagida S, *J. Phys. Chem. B*, 109, 17892 (2005).
[68] Randriamahazaka H, Fabregat-Santiago F, Zaban A, García-Cañadas J, Garcia-Belmonte G,Bisquert J, *Phys. Chem. Chem. Phys.*, 8, 1827–1833 (2006).
[69] Li Q, Luo G,Feng J, *Eletroanalysis*, 13, 359 (2001).
[70] Bisquert J,Zaban A, *Appl. Phys. A*, 77, 507 (2003).
[71] Bach U, Lupo D, Comte P, Moser J E, Weissörtel F, Salbeck J, Spreitzer H,Grätzel M, *Nature*, 398, 583 (1998).
[72] Peter L M, Duffy N W, Wang R L,Wijayantha K G U, *J. Electroanal. Chem.*, 524-525, 127 (2002).
[73] Boschloo G,Hagfeldt A, *J. Phys. Chem. B*, 109, 12093 (2005).
[74] Palomares E, Clifford J N, Haque S A, Lutz T,Durrant J R, *Journal of the American Chemical Society*, 125, 475 (2003).
[75] Bisquert, J. , Zaban A, Greenshtein M,Mora-Seró I, *J. Am. Chem. Soc.*, 126, 13550 (2004).
[76] Bisquert J, Zaban A,Salvador P, *J. Phys. Chem. B*, 106, 8774 (2002).
[77] Salvador P, González-Hidalgo M, Zaban A,Bisquert J, *The Journal of Physical Chemistry B*, 109, 15915 (2005).
[78] Ruhle S, Greenshtein M, Chen S-G, Merson A, Pizem H, Sukenik C S, Cahen D,Zaban A, *J. Phys. Chem. B*, 109, 18907 (2005).
[79] Lenzmann F, Krueger J, Burnside S, Brooks K, Grätzel M, Gal D, Rühle S,Cahen D, *J. Phys. Chem. B*, 105, 6347 (2001).
[80] Gregg B A, Pichot F, Ferrere S,Fields C L, *J. Phys. Chem. B*, 105, 1422 (2001).
[81] Wang P, Zakeeruddin S M, Comte P, Charvet R, Humphry-Baker R,Grätzel M, *J. Phys.*

Chem. B, 107, 14336 (2003).
[82] Clifford J N, Palomares E, Nazeeruddin M K, Grätzel M, Nelson J, Li X, Long N J,Durrant J R, *J. Am. Chem. Soc.*, 126, 5225 (2004).
[83] Kumara G R R A, Tennakone K, Perera V P S, Konno A, Kaneko S,Okuya M, *J. Phys. D: Appl. Phys.*, 34, 868 (2001).
[84] Zaban A, Chen S G, Chappel S,Gregg B A, *Chem. Commun.*, 22, 2231 (2000).
[85] Chappel S, Chen S G,Zaban A, *Langmuir*, 18, 3336 (2002).
[86] Diamant Y, Chen S G, Melamed O,Zaban A, *J. Phys. Chem. B*, 107, 1977 (2003).
[87] Palomares E, Clifford J N, Haque S A, Lutz T,Durrant J R, *Chem. Commun.*, 1464 (2002).
[88] Lenzmann F, Nanu M, Kijatkina O,Belaidi A, *Thin Solid Films*, 451-452, 639 (2004).
[89] Zhang X T, Liu H-W, Taguchi T, Meng R-B, Sato O,Fujishima A, *Sol. Energy Mater. Sol. Cells*, 81, 197 (2004).
[90] Fabregat-Santiago F, García-Cañadas J, Palomares E, Clifford J N, Haque S A, Durrant J R, Garcia-Belmonte G,Bisquert J, *J. Appl. Phys.*, 96, 6903 (2004).
[91] Dittrich T, Muffler H-J, Vogel M, Guminskaya T, Ogacho A, Belaidi A, Strub E, Bohne W, Röhrich J, Hilt O,Lux-Steiner M C, *Appl. Surface Science*, 240, 236 (2005).
[92] Chappel S, Grinis L, Ofir A,Zaban A, *J. Phys. Chem. B*, 109, 1643 (2005).
[93] Usami A, *Chem. Phys. Lett.*, 277, 105 (1997).
[94] Rothenberger G, Comte P,Grätzel M, *Sol. Energy Mater. Sol. Cells*, 58, 321 (1999).
[95] Kuang D, Ito S, Wenger B, Klein C, Moser J E, Humphry-Baker R, Zakeeruddin S M,Grätzel M, *J. Am. Chem. Soc.*, 128, 4146 (2006).
[96] Nishimura S, Abrams N, Lewis B A, Halaoui L I, Mallouk T E, Benkstein K D, van de Lagemaat J,Frank A J, *Journal of the American Chemical Society*, 125, 6306 (2003).
[97] Halaoui L I, Abrams N,Mallouk T E, *J. Phys. Chem. B*, 109, 6334 (2005).
[98] Mihi A, López-Alcaraz F J,Míguez H, *Appl. Phys. Lett.*, 88, 193110 (2006).
[99] Zaban A, Greenshtein M,Bisquert J, *ChemPhysChem*, 4, 859 (2003).
[100] Cao F, Oskam G, Meyer G J,Searson P C, *J. Phys. Chem.*, 100, 17021 (1996).
[101] Kambe S, Nakade S, Kitamura T, Wada Y,Yanagida S, *J. Phys. Chem. B*, 106, 2967 (2002).
[102] Nakade S, Kambe S, Matsuda M, Saito Y, Kitamura T, Wada Y,Yanagida S, *Physica E*, 14, 210 (2002).
[103] Nakade S, Saito Y, Kubo W, Kitamura T, Wada Y,Yanagida S, *J. Phys. Chem. B*, 107, 8607 (2003).
[104] Krüger J, Plass R, Grätzel M, Cameron P J,Peter L M, *J. Phys. Chem. B*, 107, 7536 (2003).
[105] Bisquert J,Vikhrenko V S, *J. Phys. Chem. B*, 108, 2313 (2004).
[106] Tiedje T,Rose A, *Solid State Commun.*, 37, 49 (1981).
[107] Tiedje T, Cebulka J M, Morel D L,Abeles B, *Phys. Rev. Lett.*, 46, 1425 (1981).
[108] Orenstein J,Kastner M, *Phys. Rev. Lett.*, 46, 1421 (1981).
[109] Michiel H, Adriaenssens G J,Davis E A, *Phys. Rev. B*, 34, 2486 (1986).
[110] Kambili A, Walker A B, Qiu F L, Fisher A C, Savin A D,Peter L M, *Physica E*, 14, 203 (2002).
[111] van de Lagemaat J,Frank A J, *J. Phys. Chem. B*, 104, 4292 (2000).
[112] van de Lagemaat J, Kopidakis N, Neale N R,Frank A J, *Phys. Rev. B*, 71, 035304 (2005).
[113] Bisquert J, *J. Phys. Chem. B*, 108, 2323 (2004).
[114] Rose A *Concepts in Photoconductivity and Allied Problems* Interscience: New York (1963).
[115] Peter L M,Wijayantha K G U, *Electrochem. Commun.*, 1, 576 (1999).
[116] van de Lagemaat J, Benkstein K D,Frank A J, *J. Phys. Chem. B*, 105, 12433 (2001).
[117] Benkstein K D, Kopidakis N, Van de Lagemaat J,Frank A J, *J. Phys. Chem. B*, 107, 7759 (2003).
[118] Anta J A, Nelson J,Quirke N, *Phys. Rev. B*, 65, 125324 (2002).
[119] Nelson J, *Phys. Rev. B*, 59, 15374 (1999).
[120] van de Lagemaat J,Frank A J, *J. Phys. Chem. B*, 105, 11194 (2001).
[121] Nelson J, Haque S A, Klug D R,Durrant J R, *Phys. Rev. B*, 63, 205321 (2001).
[122] Tachibana Y, Haque S A, Mercer I P, Durrant J R,Klug D R, *J. Phys. Chem. B*, 104, 1198 (2000).
[123] Nogueira A F, De Paoli M-A, Montaneri I, Monkhouse R, Nelson J,Durrant J R, *J. Phys.*

Chem. B, 105, 7517 (2001).
[124] Mora-Seró I, Anta J A, Garcia-Belmonte G, Dittrich T,Bisquert J, *Journal of Photochemistry and Photobiology A: Chemistry*, in press (2006).
[125] Mora-Seró I, Dittrich T, Belaidi A, Garcia-Belmonte G,Bisquert J, *J. Phys. Chem. B*, 109, 8035 (2005).
[126] Dittrich T, Mora-Seró I, Garcia-Belmonte G,Bisquert J, *Phys. Rev. B*, 73, 045407 (2006).
[127] Li B, Wang L, Kang B, Wang P,Qiu Y, *Sol. Energy Mater. Sol. Cells*, 90, 549 (2006).
[128] Tennakone K, Kumara G R R A, Kottegoda I R M, Wijayantha K G U,Perera V P S, *J. Phys. D: Appl. Phys.*, 31, 1492 (1998).
[129] Krüger J, Plass R, Cevey L, Piccirelli M, Grätzel M,Bach U, *Appl. Phys. Lett.*, 79, 2085 (2001).
[130] Krüger J, Plass R, Grätzel M,Matthieu H-J, *Appl. Phys. Lett.*, 81, 367 (2002).
[131] Papageorgiou N, Athanassov Y, Armand M, Bonhôte P, Petterson H, Azam A,Grätzel M, *J. Electrochem. Soc.*, 143, 3099 (1996).
[132] Murai S, Mikoshiba S, Sumino H, Katob T,Hayaseb S, *Chemical Communications*, 1534–1535 (2003).
[133] Kubo W, Kitamura T, Hanabusa K, Wada Y,Yanagida S, *Chem. Commun.*, 374 (2002).
[134] Wang P, Zakeeruddin S M, Moser J E,Grätzel M, *J. Phys. Chem. B*, 107, 13280 (2003).
[135] Wang P, Zakeeruddin S M, Humphry-Baker R,Grätzel M, *Chem. Mater.*, 16, 2694 (2004).
[136] Usami A, *Chem. Phys. Lett.*, 292, 223 (1998).
[137] Usami A,Ozaki H, *J. Phys. Chem. B*, (2001).
[138] Papageorgiou N, Grätzel M,Infelta P P, *Sol. Energy Mater. Sol. Cells*, 44, 405 (1996).
[139] Papageorgiou N, Barbé C,Grätzel M, *J. Phys. Chem. B*, 102, 4156 (1998).
[140] Ferber J, Stangl R,Luther J, *Sol. Energy Mater. Sol. Cells*, 53, 29 (1998).
[141] Stangl R, Ferber J,Luther J, *Sol. Energy Mater. Sol. Cells*, 54, 255 (1998).
[142] Kalaignan G P,Kang Y S, *J. Photochem. Photobiol. A: Chem.*, in press (2006).
[143] Huang S Y, Schilchthörl G, Nozik A J, Grätzel M,Frank A J, *J. Phys. Chem. B*, 101, 2576 (1997).
[144] Ni M, Leung M K H, Leung D Y C,Sumathy K, *Sol. Energy Mater. Sol. Cells*, 90, 1331 (2006).
[145] Ernst K, Engelhardt R, Ellmer K, Kelch C, Muffler H J, Lux-Steiner M C,Könenkamp R, *Thin Solid Films*, 387, 26 (2001).
[146] Könenkamp R, Dloczik L, Ernst K,Olesch C, *Physica E*, 14, 219 (2002).
[147] Lévy-Clément C, Katty A, Bastide S, Zenia F, Mora I,Munoz-Sanjose V, *Physica E*, 14, 229 (2002).
[148] Gavrilov S, Oja J, Lim B, Belaidi A, Bohne W, Strub E, Röhrich J, Lux-Steiner M C,Dittrich T, *Phys. Stat. Sol. (a)*, 203, 1024 (2006).
[149] Nanu M, Schoonman J,Goossens A, *Nano Lett.*, 5, 1716 (2005).
[150] Santato C, Ulmann M,Augustynski J, *J. Phys. Chem.*, 105, 936 (2001).
[151] Khan S U M, Al-Shahry M,Ingler W B, *Science*, 297, 2243 (2002).
[152] Torres G R, Lindgren T, Lu J, Granqvist C-G,Lindquist S-E, *J. Phys. Chem. B*, 108, 5995 (2004).
[153] Santato C, Ulmann M,Augustynski J, *Adv. Mat.*, 13, 511 (2001).
[154] Morand R, Lopez C, Koudelka-Hep M, Kedzierzawski P,Augustynski J, *J. Phys. Chem.*, 106, 7218 (2002).
[155] Solarska R, Santato C, Jorand-Sartoretti C, Ulmann M,Augustynski J, *Journal of Applied Electrochemistry*, 35, 715 (2005).
[156] Lana-Villarreal T, Bisquert J, Mora-Seró I,Salvador P, *J. Phys. Chem. B*, 109, 10355 (2005).
[157] Villarreal T L, Gómez R, González M,Salvador P, *J. Phys. Chem. B*, 108, 20278 (2004).
[158] Villarreal T L, Gómez R, Neumann-Spallart M, Alonso-Vante N,Salvador P, *J. Phys. Chem. B*, 108, 15172 (2004).
[159] Mora-Seró I, Lana-Villarreal T, Bisquert J, Pitarch A, Gómez R,Salvador P, *J. Phys. Chem. B*, 109, 3371 (2005).
[160] Granqvist C G *Handbook of Inorganic Electrochromic Materials* Elsevier: Amsterdam (1995).

[161] Etzion Y,Erell E, *Build. Environm.*, 35, 433 (2000).
[162] Hauch A, Georg A, Baumgärtner S, Opara-Krasovec U,Orel B, *Electrochim. Acta*, 46, 2131 (2001).
[163] Krasovec U O, Georg A, Georg A, Wittwer V, Joachim L,Topic M, *Solar Energy Materials and Solar Cells*, 84, 369 (2004).
[164] Georg A, Georg A,Krasovec U O, *Thin Solid Films*, 502, 246 (2006).
[165] Cummins D, Boschloo G, Ryan M, Corr D, Rao S N,Fitzmaurice D, *J. Phys. Chem. B*, 104, 11449 (2000).
[166] Bonhote P, Gogniat E, Campus F, Walder L,Grätzel M, *Displays*, 20, 137 (1999).
[167] Edwards M O M, Gruszecki T, Pettersson H, Thuraisingham G,Hagfeldt A, *Electrochem. Commun.*, 4, 963 (2002).
[168] Petterson H, Gruszecki T, Johansson L H, Norberg A, Edwards M O M,Hagfeldt A, *SID Digest of Technical Papers*, 123, (2002).
[169] Garcia-Cañadas J, Peter L M,Wijayantha K G U, *Electrochem. Commun.*, 5, 199 (2003).
[170] Bonhôte P, Gogniac E, Sophie T, Barbé C, Vlachopoulos N, Lenzmann F, Comte P,Grätzel M, *J. Phys. Chem. B*, 102, 1498 (1998).
[171] Wang Q, Zakeeruddin S M, Cremer J, Bäuerle P, Humphry-Baker R,Grätzel M, *J. Am. Chem. Soc.*, 127, 5706 (2005).
[172] Wang Q, Zakeeruddin S M, Zakeeruddin M K, Humphry-Baker R,Grätzel M, *J. Am. Chem. Soc.*, in press (2006).
[173] Trammell S A,Meyer T J, *J. Phys. Chem. B*, 103, 104 (1999).
[174] Westermark K, Tingry S, Persson P, Rensmo H, Lunell S, Hagfeldt A,Siegbahn H, *J. Phys. Chem. B*, 105, 7182 (2001).
[175] Paddon C A,Marken F, *Electrochem. Commun.*, 6, 1249 (2004).
[176] Zhang W,Li G, *Anal. Sci.*, 20, 603 (2004).
[177] Könenkamp R, *Phys. Rev. B*, 61, 11057 (2000).
[178] Kytin V,Dittrich T, *Phys. Stat. Sol. (a)*, 185, 461 (2001).
[179] Kytin V, Dittrich T, Koch F,Lebedev E, *Appl. Phys. Lett.*, 79, 108 (2001).
[180] Kytin V, Dittrich T, Bisquert J, Lebedev E A,Koch F, *Phys. Rev. B*, 68, 195308 (2003).
[181] Garcia-Belmonte G, Kytin V, Dittrich T,Bisquert J, *J. Appl. Phys.*, 94, 5261 (2003).
[182] Aurbach D, *J. Power Sources*, 146, 71 (2005).
[183] Poizot P, Laurelle S, Grugeon S, Dupont L,Tarascon J M, *J. Power Sources*, 97-98, 235 (2001).
[184] Kavan L, Kalbaci M, Zukalova M, Exnar I, Lorenzen V, Nesper R,Grätzel M, *Chem. Mater.*, 16, 477 (2004).
[185] Armstrong A R, Armstrong G, Canales J, García R,Bruce P G, *Adv. Mat.*, 17, 862 (2005).
[186] Croce F, Appetecchi G B, Persi L,Scrosati B, *Nature*, 394, 456 (1998).
[187] Amatucci G, Badway Z, Du Pasquier A,Zheng T, *Journal of the Electrochemical Society*, 148, A930 (2002).
[188] Du Pasquier A, Plitz A, Gural J, Badway Z,Amatucci G, *J. Power Sources*, 136, 160–170 (2004).
[189] Remacle F, *J. Phys. Chem. A*, 104, 4739 (2000).
[190] Franceschetti A, Williamson A,Zunger A, *J. Phys. Chem. B*, 104, 3398 (2000).
[191] Franceschetti A,Zunger A, *Appl. Phys. Lett.*, 76, 1731 (2000).
[192] Brus L E, *J. Chem. Phys.*, 80, 4403 (1984).
[193] Yu D, Wang C,Guyot-Sionnest P, *Science*, 300, 1277 (2003).
[194] Houtepen A J,Vanmaekelbergh D, *J. Phys. Chem. B*, 109, 19634 (2005).
[195] Roest A L, Kelly J J,Vanmaekelbergh D, *Appl. Phys. Lett.*, 83, 5530 (2003).
[196] Remacle F,Levine R D, *ChemPhysChem*, 2, 20 (2001).
[197] Romero H E,Drndic M, *Phys. Rev. Lett.*, 95, 156801 (2005).
[198] Yu D, Wang C, Wehrenberg B L,Guyot-Sionnest P, *Phys. Rev. Lett.*, 92, 216802 (2003).
[199] Parthasarathy R, Xiao-Min Lin X-M,Jaeger H M, *Phys. Rev. Lett.*, 87, 186807 (2001).
[200] Middleton A A,Wingreen N S, *Phys. Rev. Lett.*, 71, 3198 (1993).
[201] Roest A L, Kelly J J,Vanmaekelbergh D, *Physical Review Letters*, 89, 036801 (2002).
[202] Roest A L, Houtepen A J, Kelly J J,Vanmaekelbergh D, *Faraday Discuss.*, 125, 55 (2004).

[203] van de Lagemaat J, *Physical Review B*, 72, 235319 (2005).
[204] Yablonovitch E, *Phys. Rev. Lett.*, 58, 2059 (1987).
[205] Meseguer F,Míguez H, *IEICE Trans. Electron.*, E87, 274 (2004).
[206] Lodahl P, van Driel A F, Nikolaev I S, Irman A, Overgaag K, Vanmaekelbergh D,Vos W L, *Nature*, 430, 654 (2004).
[207] Huisman C L, Schoonman J,Goossens A, *Sol. Energy Mater. Sol. Cells*, 85, 115 (2005).
[208] Somani P R, Dionigi C, Murgia M, Palles D, Nozar P,Ruani G, *Solar Energy Materials and Solar Cells*, 87, 513 (2005).
[209] Kavan L, Zukalova M, Kalbaci M,Grätzel M, *J. Electrochem. Soc.*, 151, A1301 (2004).
[210] Fan Z,Lu J G, *J. Nanosci. Nanotech.*, 5, 1561 (2005).
[211] Huang M H, Mao S, Feick H, Yan H, Wu Y, Kind H, Weber E, Russo R,Yang P, *Science*, 292, 1897 (2001).
[212] Baxter J B,Aydil E S, *Appl. Phys. Lett.*, 86, 053114 (2005).
[213] Chae W-S, Lee S-W,Kim Y-R, *Chem. Mater.*, 17, 3072 (2005).
[214] Greene L E, Law M, Tan D H, Montano M, Goldberger J, Somorjai G,Yang P, *Nano Lett.*, 5, 1231 (2005).
[215] Baxter J B,Aydil E S, *Sol. Energy Mater. Sol. Cells*, 90, 607 (2006).
[216] Mor G K, Shankar K, Paulose M, Varghese O K,Grimes C A, *Nano Lett.*, 6, 215 (2006).
[217] Park J H, Kim S,Bard A J, *Nano Lett.*, 6, 24 (2006).
[218] Bullot J, Gallais O, Gauthier M,Livage J, *Applied Physics Letters*, 36, 986 (1980).
[219] Kim G-T, Waizmann U,Roth S, *Applied Physics Letters*, 79, 3497 (2001).
[220] Muster J, Kim G T, Krsticacute V, Park J G, Park Y W, Roth S,Burghard M, *Advanced Materials*, 12, 420 (2000).
[221] Kim G T, Muster J, Krstic V, Park J G, Park Y W, Roth S,Burghard M, *Appl. Phys. Lett.*, 76, 1875 (2000).
[222] Sun D, Kwon C W, Baure G, Richmian E, MacLean J, Dunn B,Tolbert S H, *Adv. Mat.*, 14, 1197 (2004).
[223] Yu H Y, Kang B H, Pi U H, Park C W, Choi S-Y,Kim G T, *Applied Physics Letters*, 86, 253102 (2005).
[224] Yi Cui Y, Wei Q, Park H,Lieber C M, *Science*, 293, 1289 (2001).

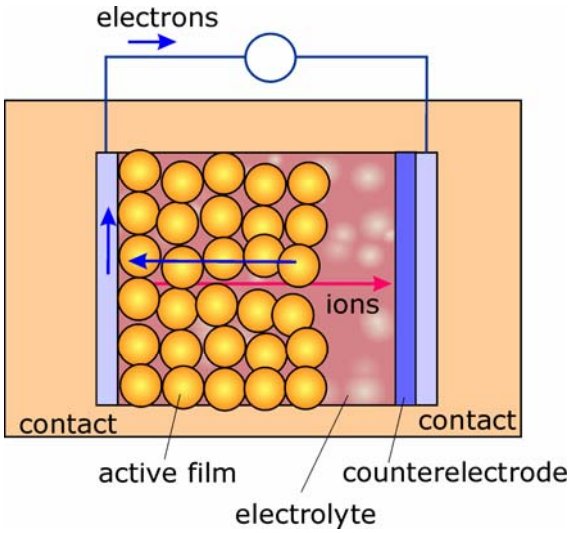

Figure 1.

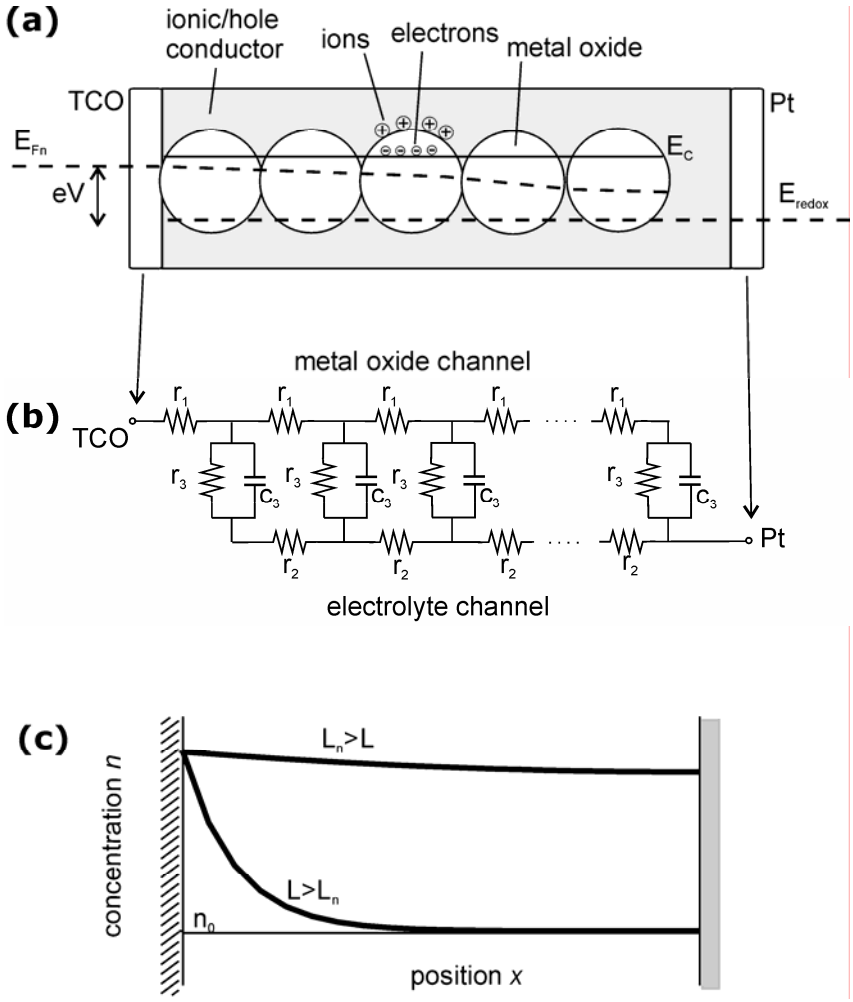

Figure 2.

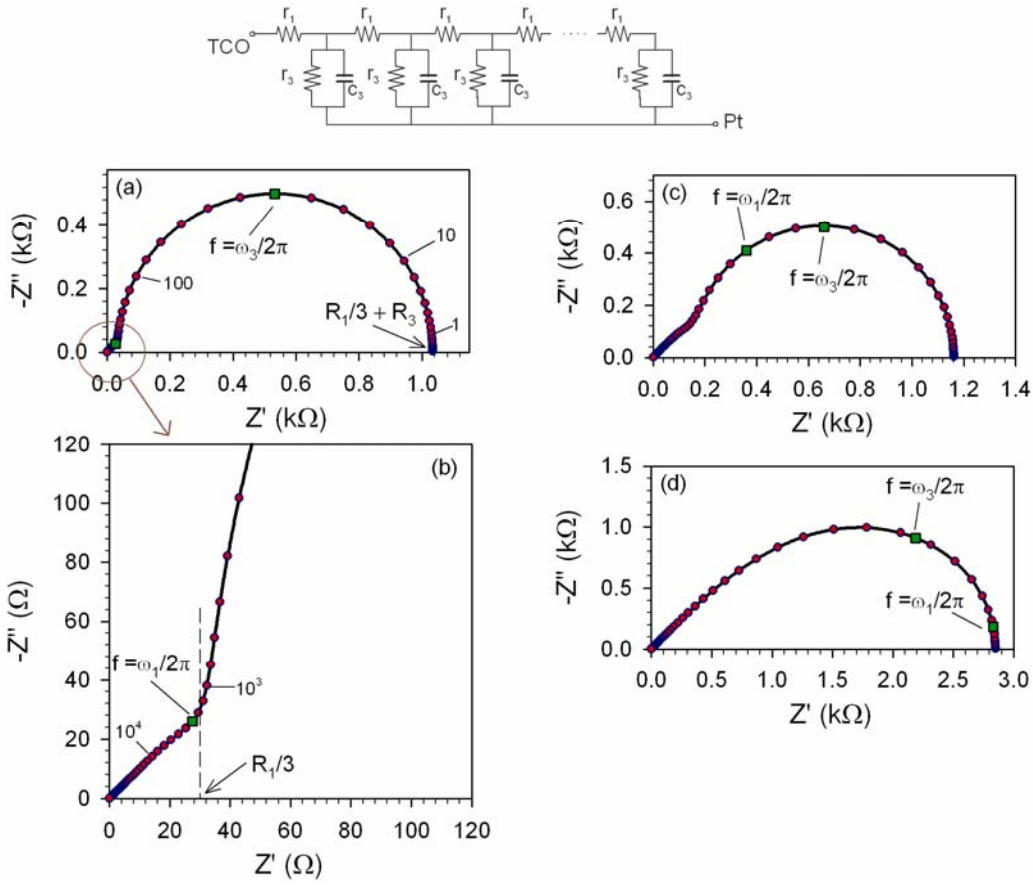
TCO
Pt
(a)
(b)
(c)
(d)
-Z'' (kΩ)
Z' (kΩ)
-Z'' (Ω)
Z' (Ω)
f =ω3/2π
f =ω1/2π
R1/3 + R3
R1/3
100
10
1
10^3
10^4

Fig. 3.

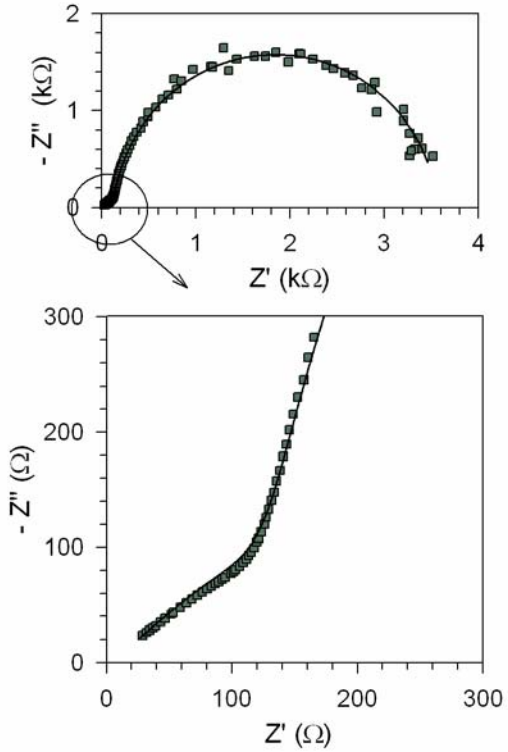
- Z'' (kΩ)
Z' (kΩ)
- Z'' (Ω)
Z' (Ω)

Fig. 4.

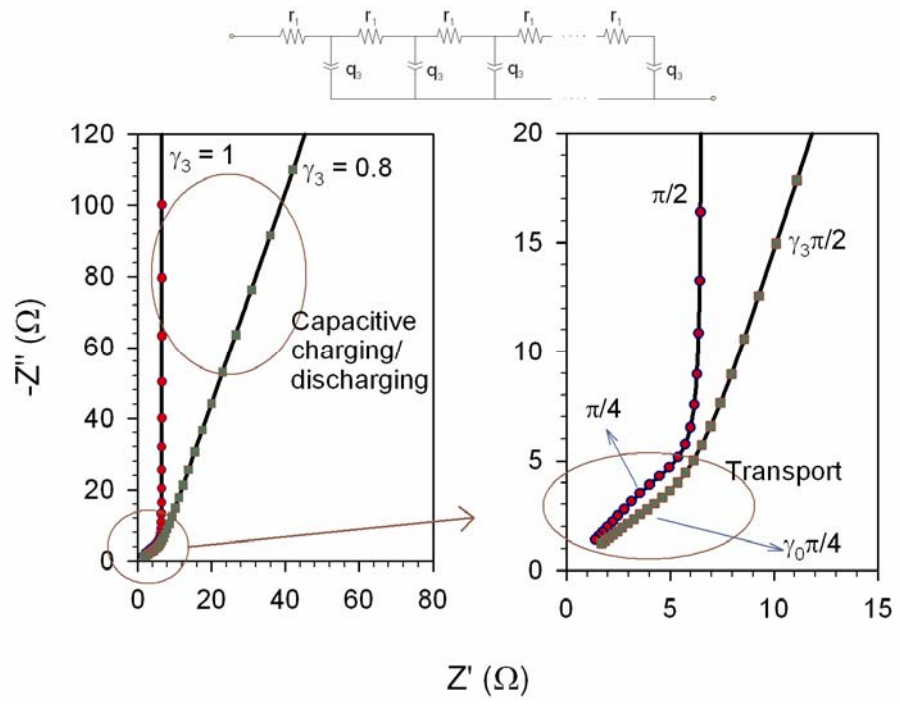

Fig. 5.

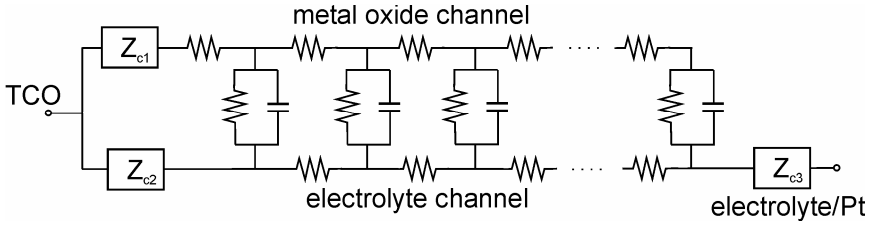

Fig. 6.

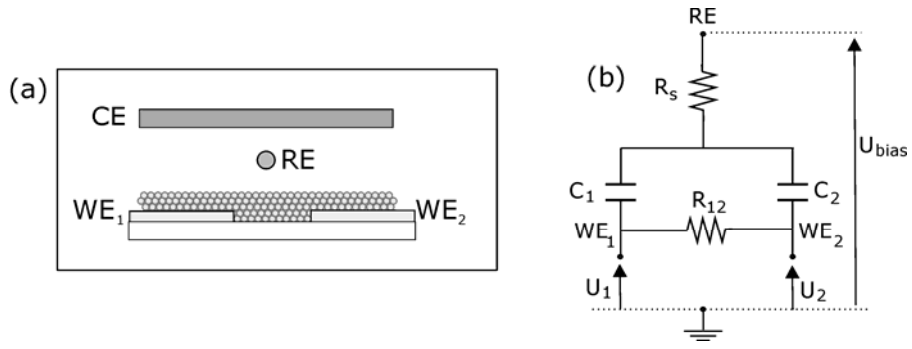

Fig. 7.

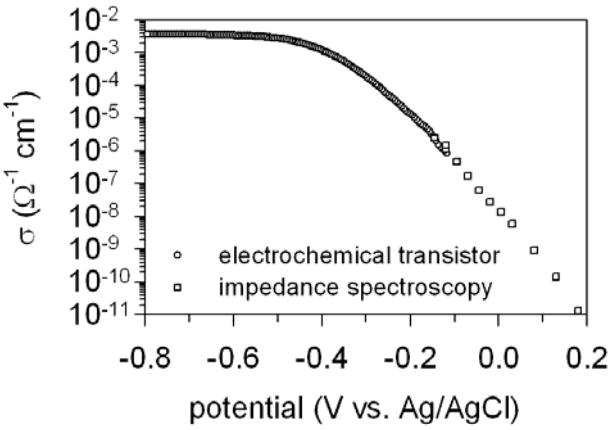
σ (Ω⁻¹ cm⁻¹)
10-2
10-3
10-4
10-5
10-6
10-7
10-8
10-9
10-10
10-11
electrochemical transistor
impedance spectroscopy
-0.8
-0.6
-0.4
-0.2
0.0
0.2
potential (V vs. Ag/AgCl)

Fig. 8.

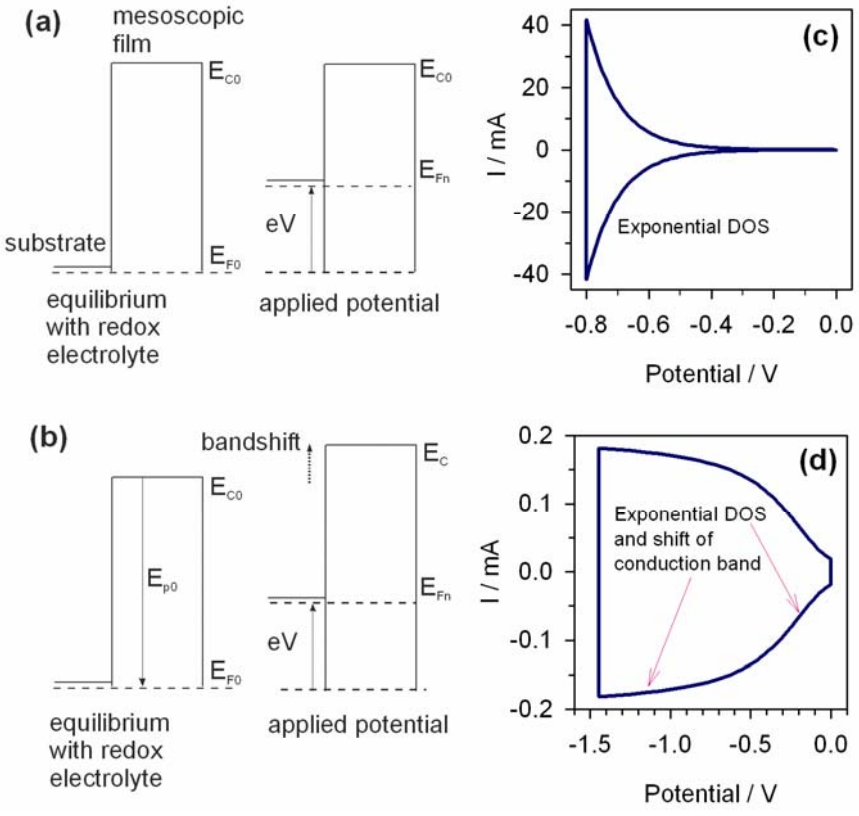
(a)
mesoscopic film
E_C0
substrate
E_F0
equilibrium with redox electrolyte
E_C0
E_Fn
eV
applied potential
(c)
40
20
0
-20
-40
I / mA
Exponential DOS
-0.8
-0.6
-0.4
-0.2
0.0
Potential / V
(b)
bandshift
E_C0
E_p0
E_F0
equilibrium with redox electrolyte
E_C
E_Fn
eV
applied potential
(d)
0.2
0.1
0.0
-0.1
-0.2
I / mA
Exponential DOS and shift of conduction band
-1.5
-1.0
-0.5
0.0
Potential / V

Fig. 9.

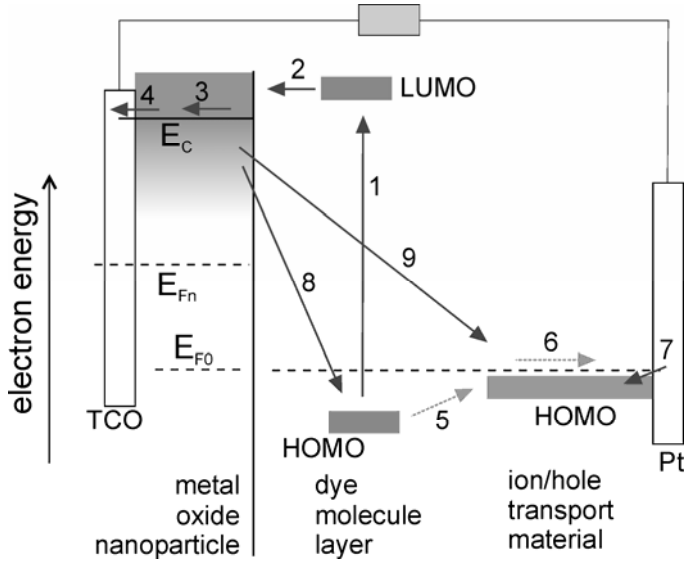
2
LUMO
4
3
E_C
1
9
8
E_{Fn}
E_{F0}
6
7
5
HOMO
HOMO
TCO
Pt
electron energy
metal
oxide
nanoparticle
dye
molecule
layer
ion/hole
transport
material

Fig. 10.

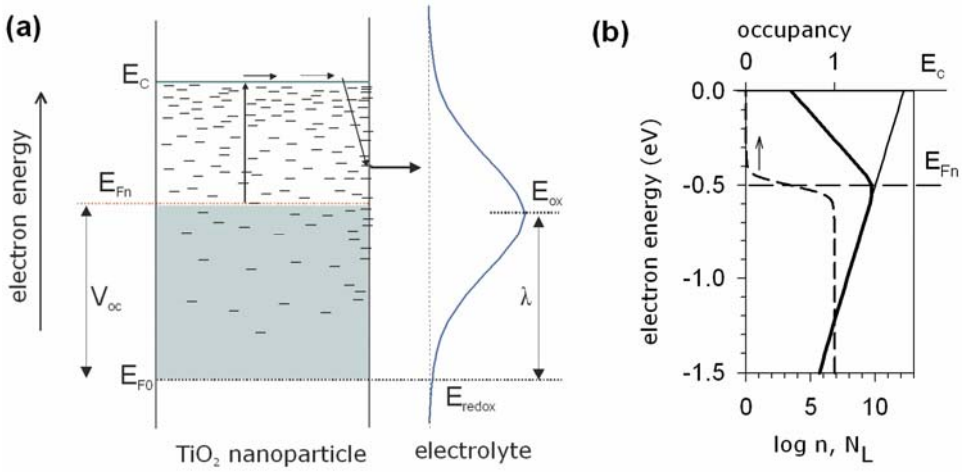
(a)
E_C
E_{Fn}
V_{oc}
E_{F0}
electron energy
E_{ox}
λ
E_{redox}
TiO_2 nanoparticle
electrolyte
(b)
occupancy
0
1
E_C
0.0
-0.5
-1.0
-1.5
E_{Fn}
electron energy (eV)
0
5
10
log n, N_L

Fig. 11.

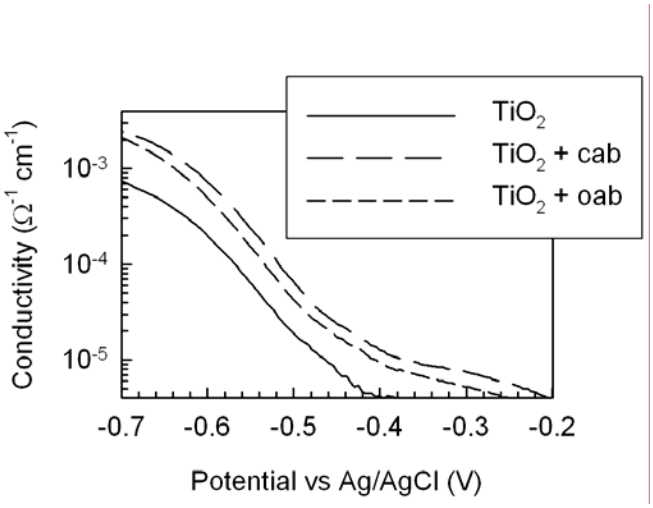

Figure 12.

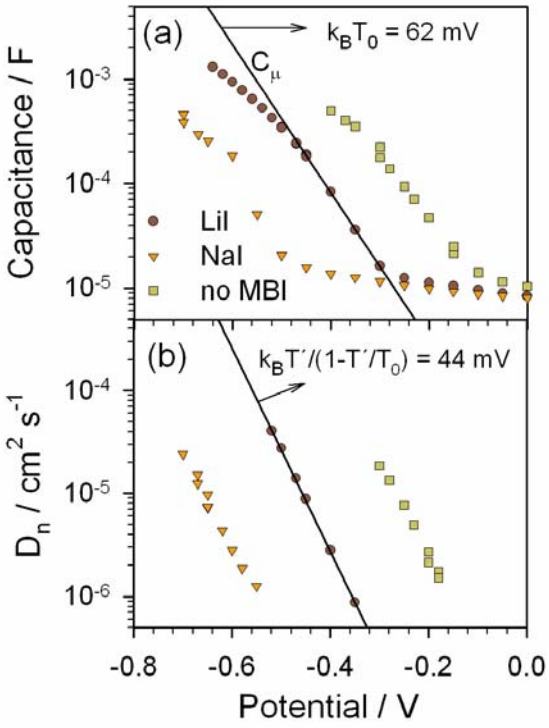

Figure 13.

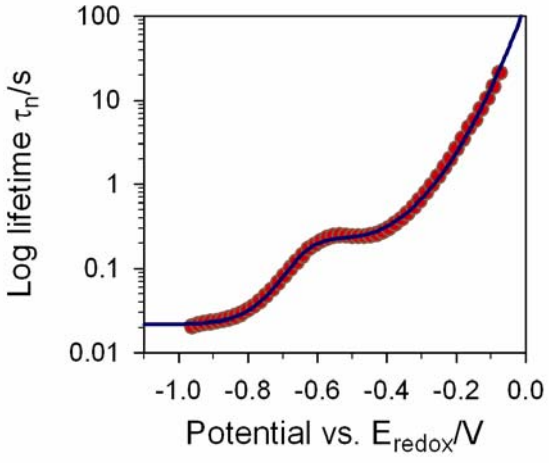

Fig. 14.

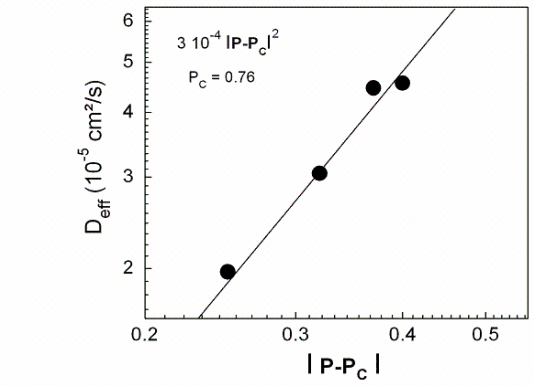

Figure 15.

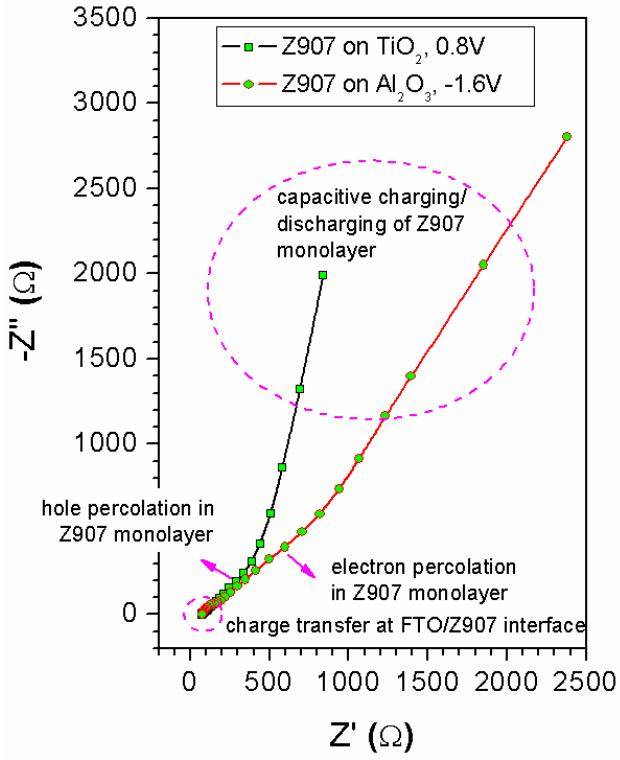
Z907 on TiO2, 0.8V
Z907 on Al2O3, -1.6V
capacitive charging/
discharging of Z907
monolayer
hole percolation in
Z907 monolayer
electron percolation
in Z907 monolayer
charge transfer at FTO/Z907 interface
-Z'' (Ω)
Z' (Ω)
0
500
1000
1500
2000
2500
3000
3500

Fig. 16.